LAMONT-DOHERTY GEOLOGICAL OBSERVATORY
OF COLUMBIA UNIVERSITY
Palisades, New York 10964

OBSERVATIONS OF CURRENTS IN THE ARCTIC OCEAN

by

Robert L. Bernstein

January, 1972

Technical Report No. 7
Contract N-00014-67-A-0108-0016 with
the Office of Naval Research
Task Number NR 307-320/1-6-69
(415)

LAMONT-DOHERTY GEOLOGICAL OBSERVATORY
OF COLUMBIA UNIVERSITY
Palisades, New York 10964

OBSERVATIONS OF CURRENTS IN THE ARCTIC OCEAN

by
Robert L. Bernstein
January, 1972

Technical Report No. 7
Contract N-00014-67-A-0108-0016 with
the Office of Naval Research
Task Number NR 307-320/1-6-69
(415)

ABSTRACT

Observations of Currents in the Arctic Ocean

Robert L. Bernstein

An array of current meters was installed and operated for three months at Ice Island T-3, at 85°N, 95°W in the Arctic Ocean. Current meters were placed at three sites at 40m and 70m depths, with signal outputs all wired to a common recording system. The drift motion of T-3 can be eliminated from the records using frequent precise satellite navigation fixes. All records show predominant 12 hour period inertial currents, superimposed on lower frequency transient currents, which occur during intervals of rapid ice drift. The transient currents, at 40m in an upper layer veer to the right of the ice drift direction, while currents in the lower layer at 70m veer to the left. The observed ice drift and currents are consistent with the theory of elementary currents first advanced by Ekman, and with a recent theory by Pollard.

The inertial currents have constant phase and amplitude which only change during intervals of ice displacement, suggesting the local generation of these currents in the upper levels of the ocean.

The kinetic energy power spectrum derived from the current meter time series shows an even fall-off of energy proportional to the -5/3 power of frequency. This fall-off is interrupted by an energy peak at the 12 hour inertial period. The -5/3 fall-off suggests that energy is fed in at large scales and long periods ($>$ 2-3 days) and dissipates in an energy cascade through smaller scales and high frequencies.

The magnitude of the surface stress which the moving ice cover

exerts on the underlying ocean has been estimated by a new method. From the decay of transient currents under a non-moving ice cover, a simple theory gives a stress value around 0.7 dynes/cm^2, for 10 cm/sec of relative velocity between the ice and the water underneath.

TABLE OF CONTENTS

LIST OF FIGURES

LIST OF TABLES

INTRODUCTION

Introductory Remarks

A complete understanding of ocean dynamics requires detailed observations of ocean currents over a wide range of space and time scales. Observation of transient currents requires refined current sensors mounted on stable platforms. Recent developments of the Savonious rotor current meter and the digital magnetic tape recorder provide highly suitable instrumentation for this purpose. The drifting ice stations on the Arctic ocean provide stable platforms for mounting the current meters on rigid inverted masts. The present study describes measurements of transient ocean currents with a three-dimensional array of current meters with horizontal aperture of 370m and vertical aperture of 70m. The data were all recorded on a single magnetic tape providing a common time base not available in any previous deep ocean current observations. The common time base allows precise comparisons between instruments. The stable ice mounting avoids the spurious oscillations and noise injected by buoy mountings in other oceans. These data are therefore unique in their phase precision and lack of high-frequency noise. Wave motion and cable oscillation have been eliminated in this experiment.

Historical Background

Scientific observations of wind and weather, ice movement, and the underlying Arctic ocean dates back to the earliest explorers of this harsh environment. The historic drift of the "Fram" by NANSEN (1902) yielded results which stand in many ways unimproved upon.

Other similar expeditions followed Nansen.

Beginning in the 1930's Soviet workers began long-term occupations of drifting ice floes which continue to the present. Following the end of World War II, U.S. Air Force and Navy interests resulted in the occupation of a number of ice stations. Most permanent of these is Fletcher's Ice Island (T-3). Unlike ice floes which are generally only a few meters thick, T-3 is many times thicker. It is a piece of glacial ice, probably broken off from Ellesmere Island. The extra thickness keeps the ice intact so that permanent stations can be maintained. T-3 drifts in a large, geostrophic clockwise circulation, called the Beaufort Gyre, contained in the Canadian Basin of the Arctic Ocean (figure 1). T-3 has been almost continuously manned since 1950, and during this time it has completed nearly three circuits around this gyre.

The drift of T-3 and the rest of the permanent ice cover in the Canadian Basin is related to the mean annual atmospheric pressure distribution of the region.

General Drift of the Arctic Pack Ice

A high pressure system (in the Northern Hemisphere) is associated with a geostrophic wind system causing clockwise circulation around the center of the high. The direction toward which the wind blows is generally almost parallel to the pressure isobars, except near the surface. There, friction and the Coriolis force interact in what is termed an Ekman boundary layer. The resulting wind near the surface blows outward from the high, at an angle approximately 30° to the direction of the isobars (figure 2a). For a low pressure system

(figure 2b), the geostrophic circulation is counter-clockwise, with surface wind blowing in toward the center of the low.

In the Arctic, ice usually drifts at some acute angle (30° to 45°) to the right of the direction of the surface wind vector $\mathbf{V_s}$ (figure 3), as was first observed by Nansen. From many observations of Soviet ice stations, ZUBOV (1945) noted the resulting parallel alignment of pressure isobars and ice drift tracks. FELZENBAUM (1958) developed a theory yielding parallel alignments by considering a model incorporating wind and water stress forces on the ice, along with Coriolis force (independent of latitude), and pressure gradient force, while neglecting any large scale resistance to strain within the ice cover.

Zubov's result has been considered valid for monthly and longer time scales. Recent advance in navigation has allowed improved resolution of ice drift tracks. Results from the experiment to be described here showed that the drift track generally conformed to the isobar pattern down to a one day time scale.

From Felzenbaum's fifteen year mean annual sea level pressure field over the Western Arctic (figure 4), CAMPBELL (1965) has calculated surface wind stress. He then calculated ice drift from this stress field, incorporating the effects of air and water stress, actual Coriolis variation with latitude, internal ice resistance to strain, and pressure gradient forces. The resulting ice drift was not quite parallel to the isobars, and would produce a convergence of ice in the center of the Beaufort Gyre. One of his typical cases is shown in figure 5. The existence of suce a convergence has yet to be demonstrated. COACHMAN (1969) has illustrated that the drift tracks of numbers of ice stations in the Beaufort Sea do roughly parallel the isobars of

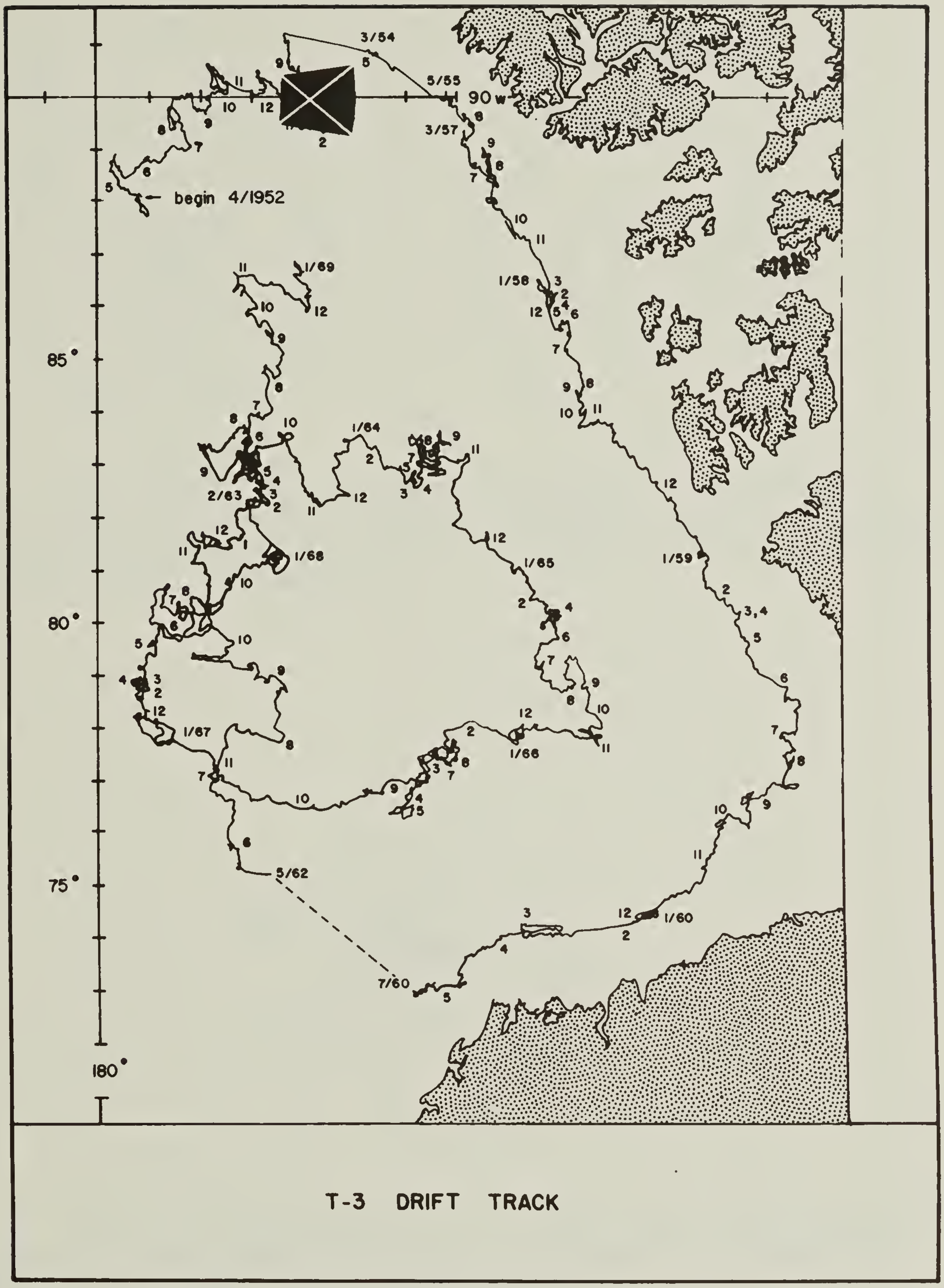

Fig. 1. Drift track of T-3 from 1952 to 1969. Insert shows area covered in progressive vector diagram, figure 17.

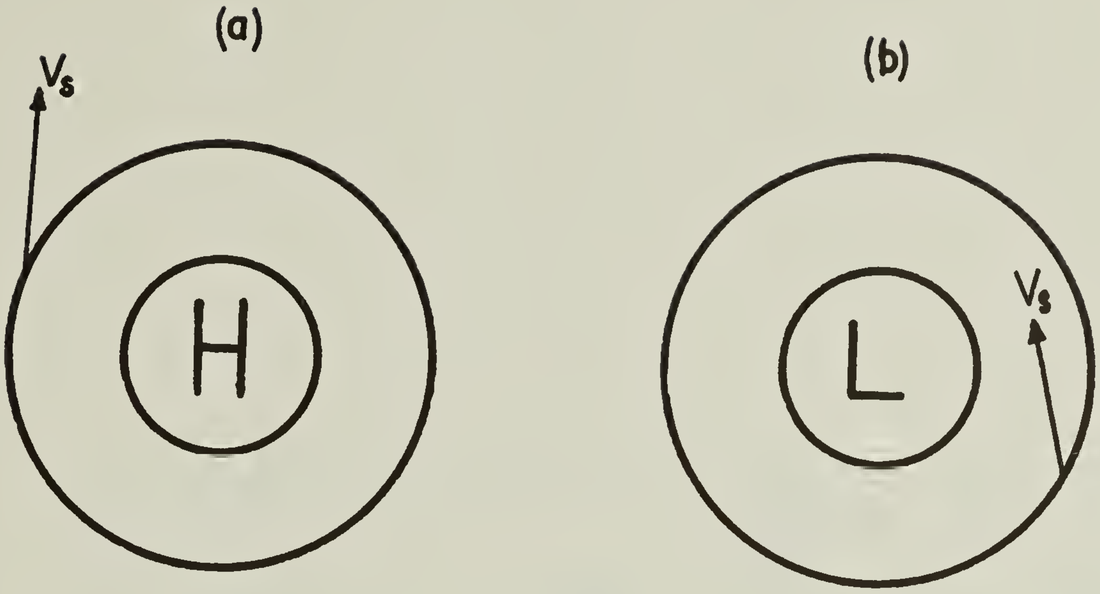

Fig. 2. (a) Clockwise geostrophic flow around a high-pressure system, with surface wind V_s blowing outward 30° from the isobars. (b) Counter-clockwise flow around a low-pressure system, V_s blowing inward 30° from the isobars.

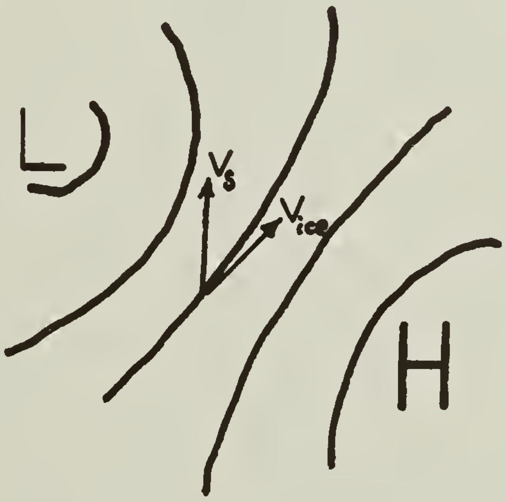

Fig. 3. Ice drifts approximately 30° to the right (in Northern Hemisphere) of the surface wind V_s , resulting in near-parallel alignment of ice drift track and isobars.

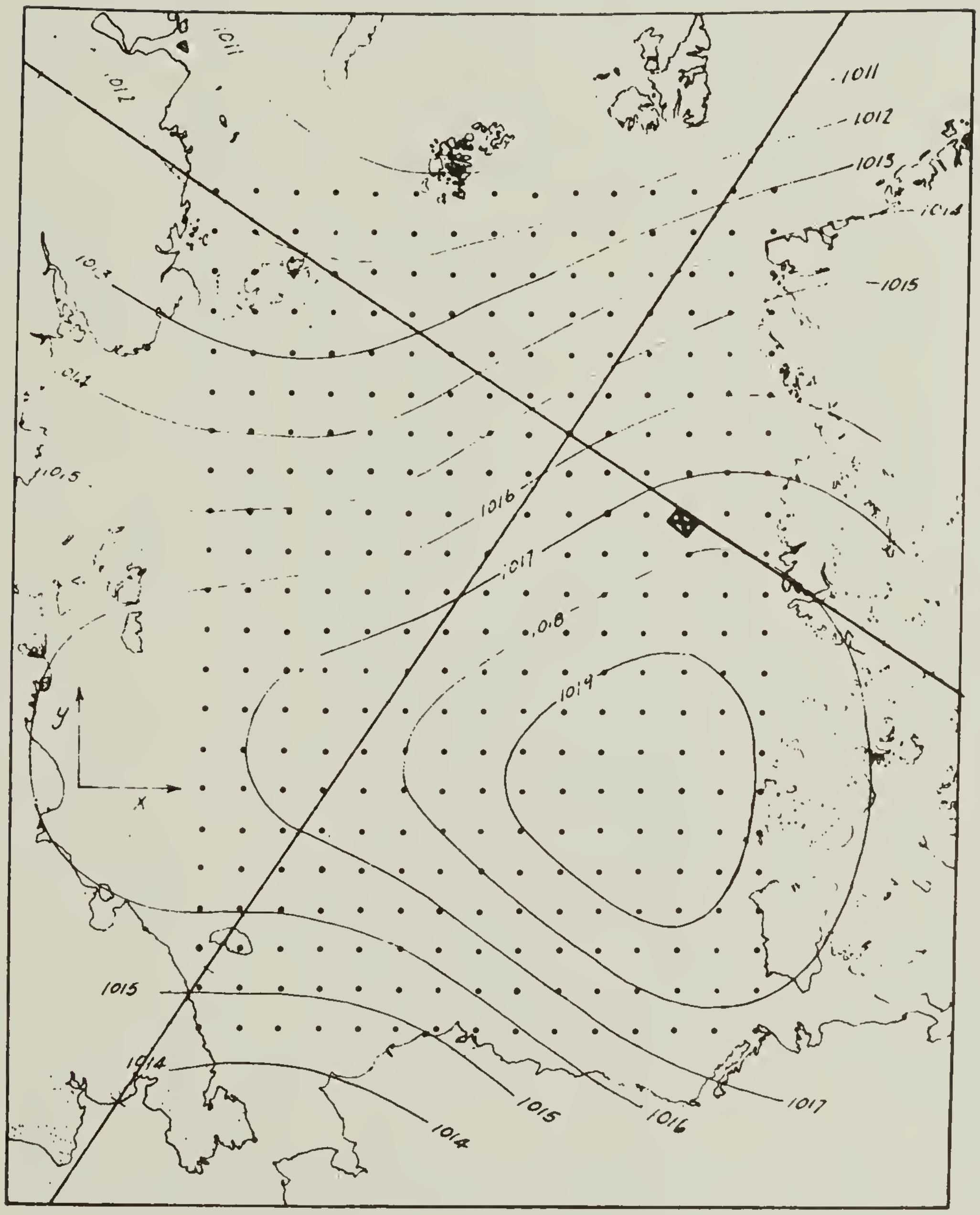

Fig. 4. Fifteen-year mean annual sea level pressure field over the Western Arctic. From CAMPBELL (1965), after FELZENBAUM (1958). Pressure is in millibars. Insert shows area covered by figure 17.

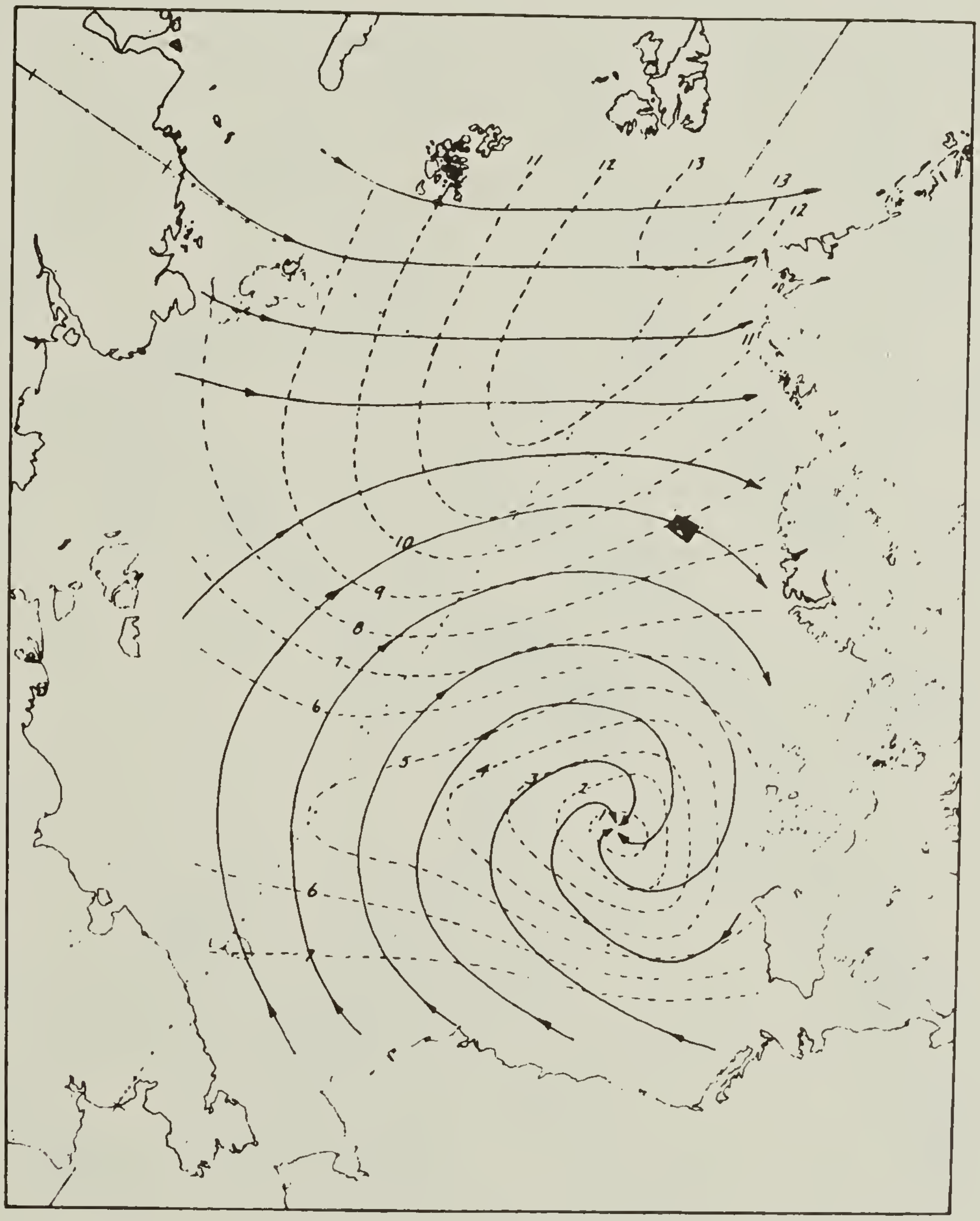

Fig. 5. Theoretical ice drift in the Arctic, incorporating effects of air and water stress, actual Coriolis variation with latitude, internal ice resistance to strain, and pressure gradient forces. From CAMPBELL (1965). Solid lines are ice velocity streamlines; dash lines are isotachs in cm/sec. Insert shows area covered by figure 17.

Fig. 6. Drift tracks of several ice stations in the Beaufort Sea trace out the isobars of the mean anticyclonic system over the region. From COACHMAN and BARNES (1961). Insert shows area covered by figure 17.

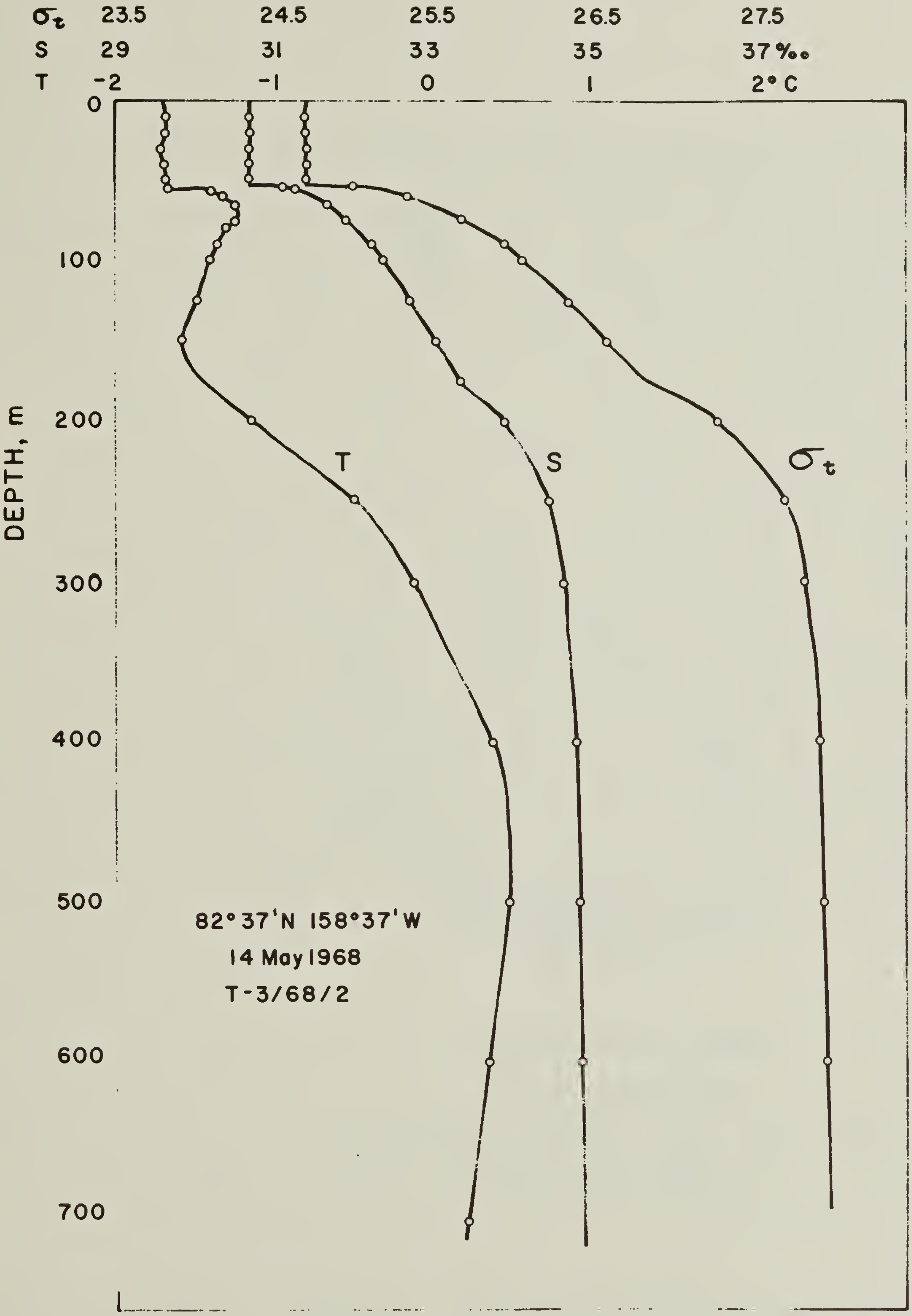

Fig. 7. Typical Arctic Ocean profile of temperature (T), salinity (S), and density (σ_t). Note the highly stratified layer above 250m, atop a nearly uniform layer. The upper 50m (upper mixed layer) has uniform density resulting from surface action. (K. HUNKINS, personal communication).

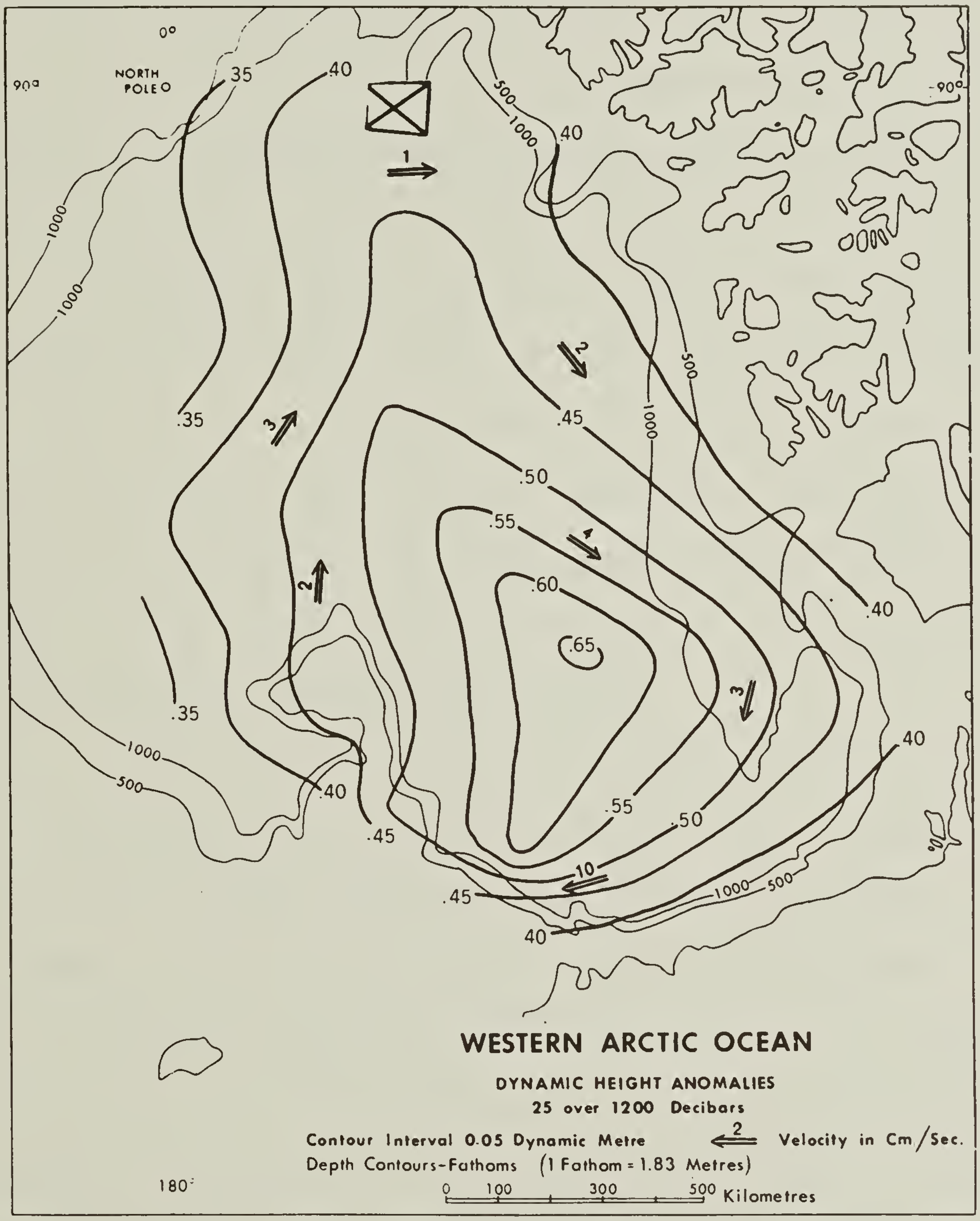

Fig. 8. Dynamic topography of the Western Arctic Ocean, showing convergence of surface water in the center of the Beaufort Gyre. From COACHMAN and BARNES (1961). Insert shows area covered by figure 17.

the mean anticyclonic system centered at 80° N, 140° W (figure 6).

We now turn attention from the ice cover to the ocean underneath. The top 50m of the Arctic Ocean is uniform, being well-mixed by surface action, and is referred to as the upper mixed layer (figure 7). Below this, a continuously stratified layer extends to a depth of 250m, which in turn overlies a nearly uniform lower layer extending to the bottom. COACHMAN and BARNES (1961) have examined hydrographic information collected from many sources over many years from the Western Arctic. The dynamic topography which they constructed from this data (figure 8) revealed a lens of surface water in the center of the gyre, associated with a clockwise geostrophic gyre in these surface waters. This gyre is quite similar to the geostrophic circulation accompanying the mean atmospheric pressure distribution.

The fact that the upper ocean geostrophically follows the atmospheric circulation may not be too surprising. Such a result is predictable from the EKMAN (1905) theory of elementary currents. According to Ekman, a stress at the surface causes a net transport of surface waters at a direction 90° to the right of the stress. For the observed clockwise ice drift of the Beaufort Gyre, this would result in a convergence of surface waters at the center of the gyre, as seen by Coachman and Barnes. This convergence must be associated with a clockwise geostrophic circulation of the water in the Beaufort Gyre.

One of the main results of the present experiment is a detailed description of the manner in which water converges toward the center of the gyre. The results will show that transient currents are set up by storms moving the ice, which in turn stresses the water. These transient currents, which only last for the duration of the storm, are

shown to follow the Ekman theory, even on a time scale as short as one day. Individual storms tend to move the ice in apparently random directions, so that it is only over a period of years that the weak Polar high pressure system manifests its presence with the ice and also the surface waters, causing net circulation around the gyre.

THE EXPERIMENT

The Current Meter Array

Ice Island T-3 provides a highly stable platform for conducting oceanographic studies. The island is roughly 10km by 6km and 30m thick, entirely surrounded by pack ice 3m thick (figure 9). Other advantages accrue from various independent operations on T-3. The U.S. Weather Bureau collects wind and atmospheric data, while the University of Washington has a program involving hydrographic casting. Lamont-Doherty Geological Observatory supplies satellite and celestial navigation, bottom and subbottom profiling, gravity and magnetics measurements.

In this setting, current meter studies have been undertaken for several years. The present experiment is an attempt to improve or extend previous results. The current meters used were externally recording (Marine Advisors, Model Q-9) with all telemetry cabling brought to a single recording site. The Savonius rotor speed sensor and direction vane sensor are of a design which has become almost standard in oceanography for the past decade. Here data were recorded on a digital magnetic tape system (Hewlett-Packard 2012D) and a multipoint chart recorder.

All current meter outputs were sampled once a minute. This is considered to be high enough to avoid aliasing of speed channel measurements. Electronic circuitry at the recording site integrates speed measurements over a 30-second interval. Direction measurements are subject to some degree of aliasing because these measurements are only integrated over a 5-second interval. The resulting vane flutter

in the measurements is usually confined to ± 5° or less.

Aside from a few drogue-type current measurements (HUNKINS, 1966, BROWNE and CRARY, 1958), all previous investigators in the Arctic have used current meters with internal compasses for referencing the direction of currents. Compasses are often unreliable in high latitudes. In the present experiment, directions were referred to the ice itself. The current meters were suspended on aluminum pipe in an inverted mast technique. The pipe rigidly controls the orientation of the current meter. The orientation is determined once and then assumed to remain constant.

All oceanographic work at T-3 is done on Colby Bay, a stable piece of pack ice permanently attached to the island and much thinner than the island itself. Current meters were placed at depths of 40m and 70m. The choice of depths was based on several considerations. From hydrocast data (figure 7) the depth to the base of the upper mixed layer was determined to be 50m. Since the draft of the ice island is 30m, 40m was the logical choice for measurements in this upper layer, in order to minimize any effect of the ice island wake on the current. Previous experience with profiling the upper 200m with current meters had revealed an interesting jet-like current at around 70m (figure 10). Thus the choice of 70m, below the upper mixed layer, was made. Deeper measurements were of course desirable but difficult to obtain because of the pipe suspension system. One current meter was placed at 100m, but failed to operate.

In earlier studies at T-3, current meters were placed in vertical arrays. In the present experiment, some current meters were placed at the same depth but horizontally separated (figure 11), in order to

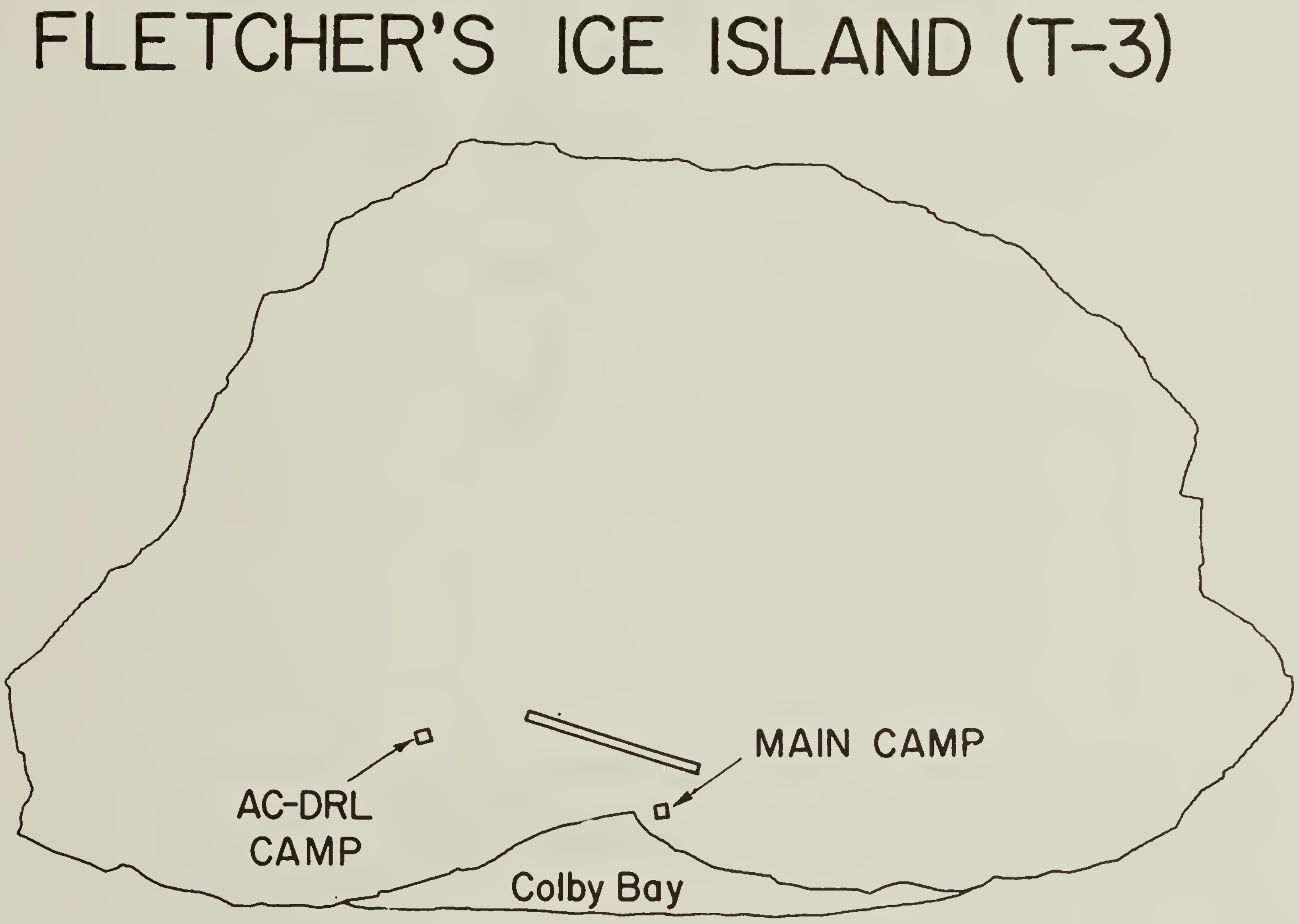

Fig. 9. Outline of Fletcher's Ice Island (T-3). The island is a 30m thick piece of glacier ice, surrounded by 3m thick pack ice. All oceanographic work is done on Colby Bay, a protected section of pack ice attached to the island. Runway near main camp is 1.5 km long.

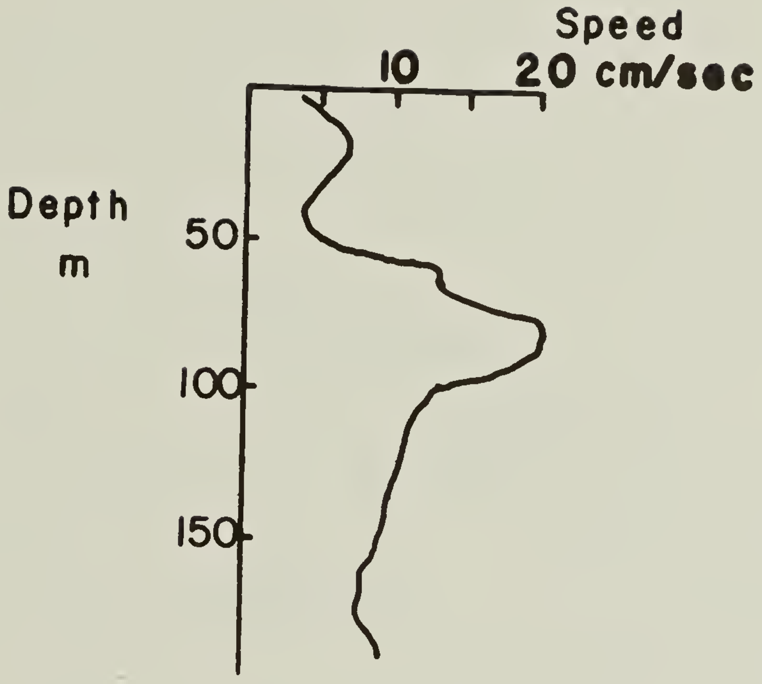

Fig. 10. Vertical profile of relative current speed taken at T-3 in May 1968. Note intensification of current centered around 70m. Current direction is toward 160°T except above 30m. (K. HUNKINS, personal communication).

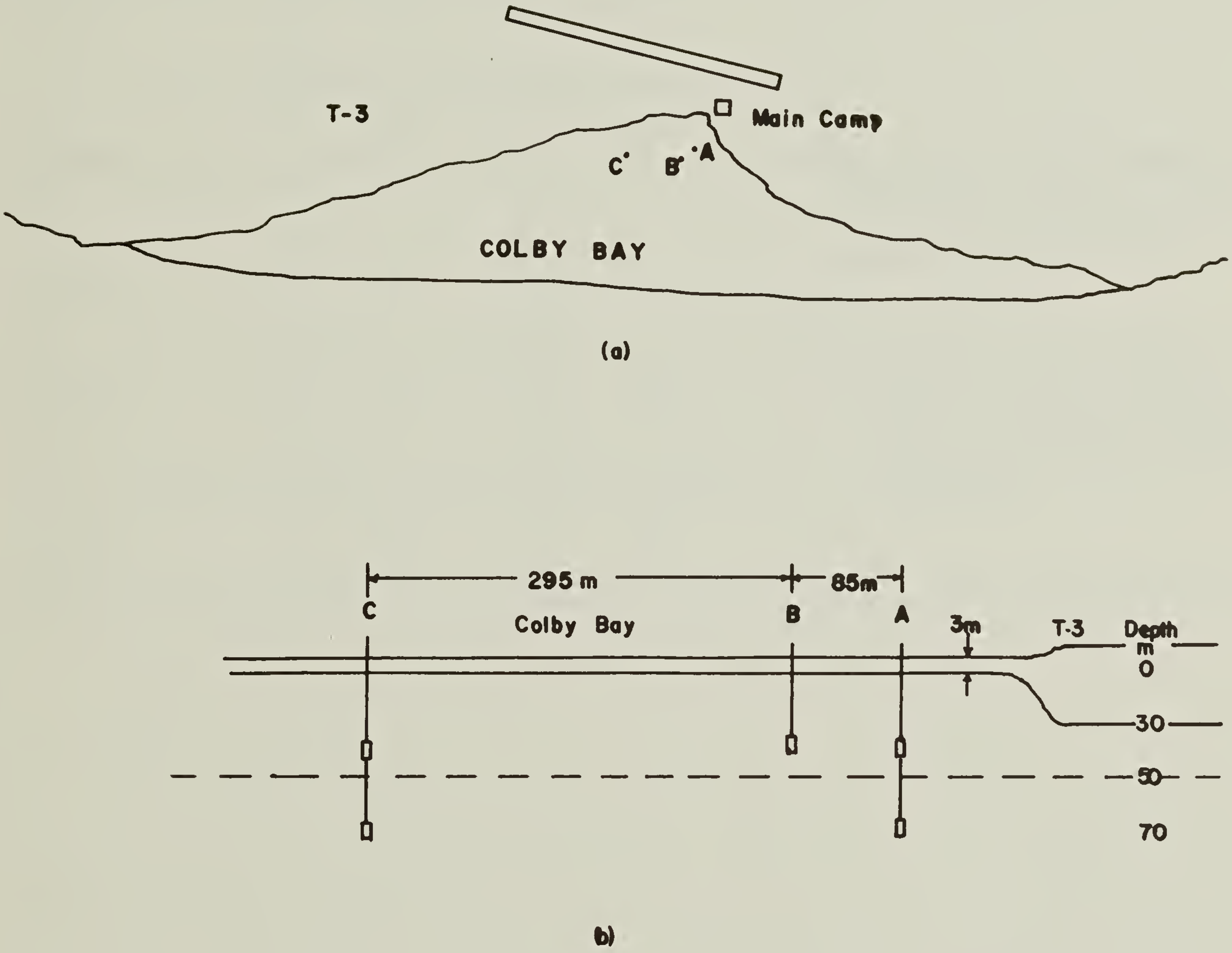

Fig. 11. Current meter array operated at T-3 for the present experiment. (a) Plan view with Masts A, B, and C located on Colby Bay. For scale, the runway shown on the map is 1.5 km long. (b) Masts A and C each held two current meters at 40m and 70m depths. Mast B held one current meter at 40m depth.

TABLE 1 Current Meter Characterics

Site	Current Meter	Depth (m)	Days of reliable record (from 0000Z 25 Nov. 1970	Comments
A	A70	70	87	
	A40	40	70	
B	B40	40	-----	Direction vane sticks-- only reliable in currents above 10 cm sec^{-1}
C	C70	70	87	C70 and C40 appear slightly more reliable than A70, A40 in small currents
	C40	40	70	

examine horizontal versus vertical coherence of currents. The main characteristics of the various current meters and the records obtained from them are listed in Table 1. Three separate masts were installed at sites A, B, C, with separations of 85m, 295m, and 370m between masts. The locations of sites A and B were dictated by operational constraints. Site C was placed as far from A and B as possible, again limited by practical considerations. Unfortunately the current meter at site B developed a sticky vane and was not useful when current speeds were much less than 10cm/sec. Certain short stretches of the record from current meter B40 are useful and were examined for high frequency structure. The main advantage however, in having records at sites A and C from the same depths (40m, 70m) was improved confidence in the working and reliability of any one current meter. Later, when current meters began to fail, duplication served to extend the useful total length of the record.

Navigation

Most reported current observations in the Arctic were conducted prior to the introduction of the Transit satellite navigation system. From the moving platform of a drifting ice station, current meters are only measuring currents relative to the ice station. In order to convert a relative current vector to an absolute current vector (relative to a fixed point on the ocean bottom, for example), one must vectorially add the ice platform's drift velocity to the relative current vector. The determination of ice drift velocity for this conversion places great demands on navigation fix accuracy, and on the frequency with which fixes are made. Using only celestial navigation

it was often impossible for HUNKINS (1967) to say whether currents observed at ice island T-3 were the result of absolute currents, or of island motions towing current meters through the water. The present experiment has the advantage of frequent, accurate satellite navigation fixes. Thus the conversion of the relative current velocities into absolute velocities becomes possible. Fixes generally were obtained every two hours, accurate to better than 400m.

RESULTS OF DATA ANALYSIS

Ice Drift and Wind

As stated previously, the ice cover drifts mainly under the influence of the surface wind, following Nansen's rule. The ratio of ice drift speed to wind speed (as measured at 10m elevation) is approximately 1:50. The ice drifts in a direction about 30^{o} to the right of the direction toward which the wind blows. To show the degree to which T-3's drift followed Nansen's rule during the present experiment, the hourly averaged wind vectors have been rotated clockwise through 30^{o} and divided in magnitude by a factor of 50. The east and north components of this vector is compared with the two components of the ice island drift velocity in figure 12. The ice drift velocity was derived from the satellite navigation fixes, and filtered to suppress the noise associated with fix inaccuracies. Variations in ice velocity with periods less than 6 hours were filtered out.

Representation of Currents by Components

Ocean currents are vector quantities which change with time. Horizontal currents relative to a moving platform were recorded at T-3. The relative current vectors must first be corrected for the motion of T-3 by the vectorial subtraction of T-3's drift.

A horizontal current vector may be described by speed and direction or else by components, north and east. Components are more convenient to work with when vector addition and subtraction are required. All current speed and direction records were converted to east and north velocity components, with components linearly inter-

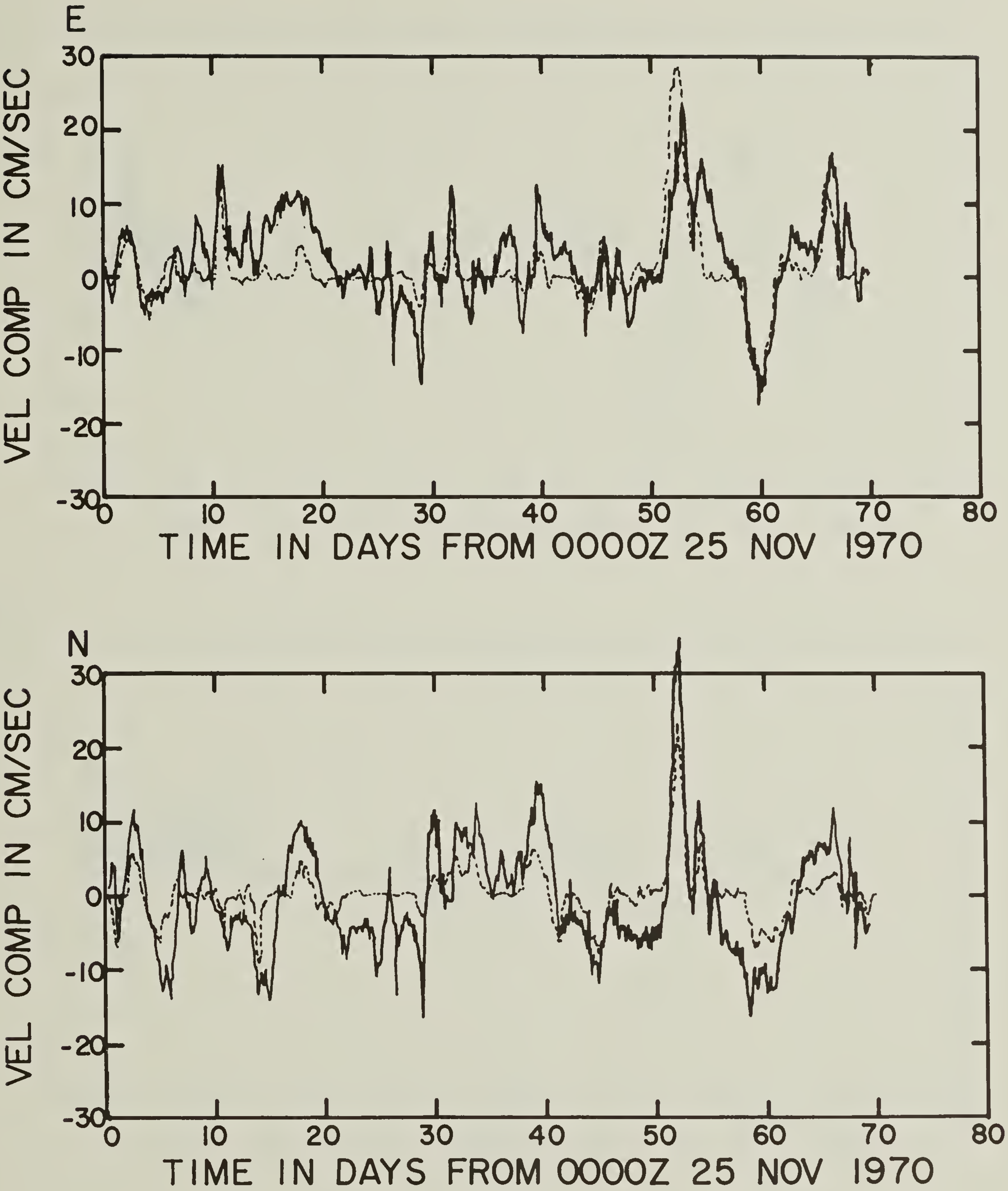

Fig. 12. Comparison of wind velocity (solid line) and ice drift velocity (dash line). Wind velocity vector (pointing in direction toward which wind blows) has been rotated 30° clockwise and divided in magnitude by a factor of 50 before taking east and north components. Ice drift velocity derived from satellite navigation fixes. Nansen's rule is followed where the two curves coincide.

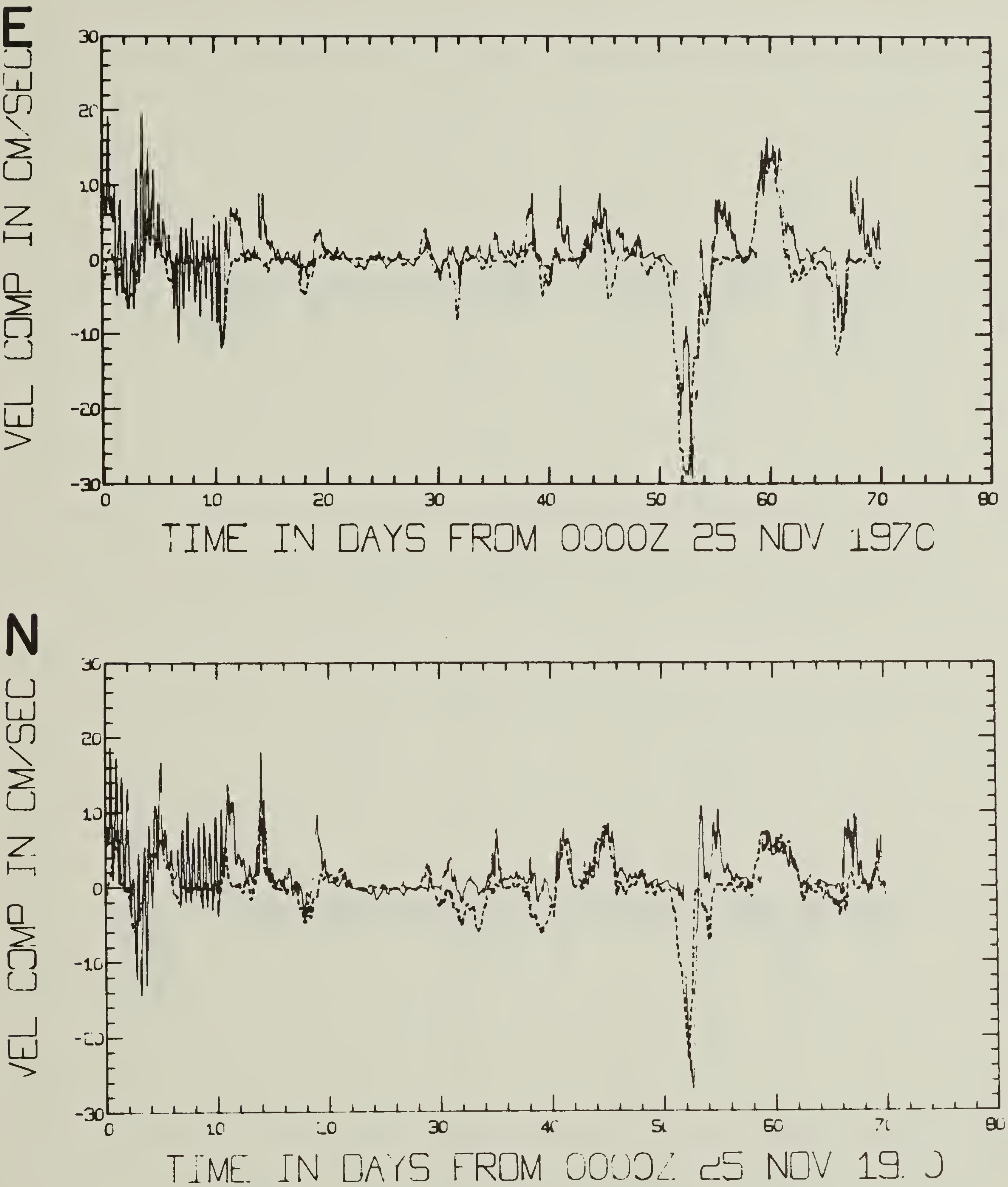

Fig. 13. Relative currents (solid line) from 40m current meter on Mast C. Upper graph gives east component of current, lower graph gives north component. Negative of T-3's velocity (dash line) also shown. Departure of solid line from dash line gives absolute current.

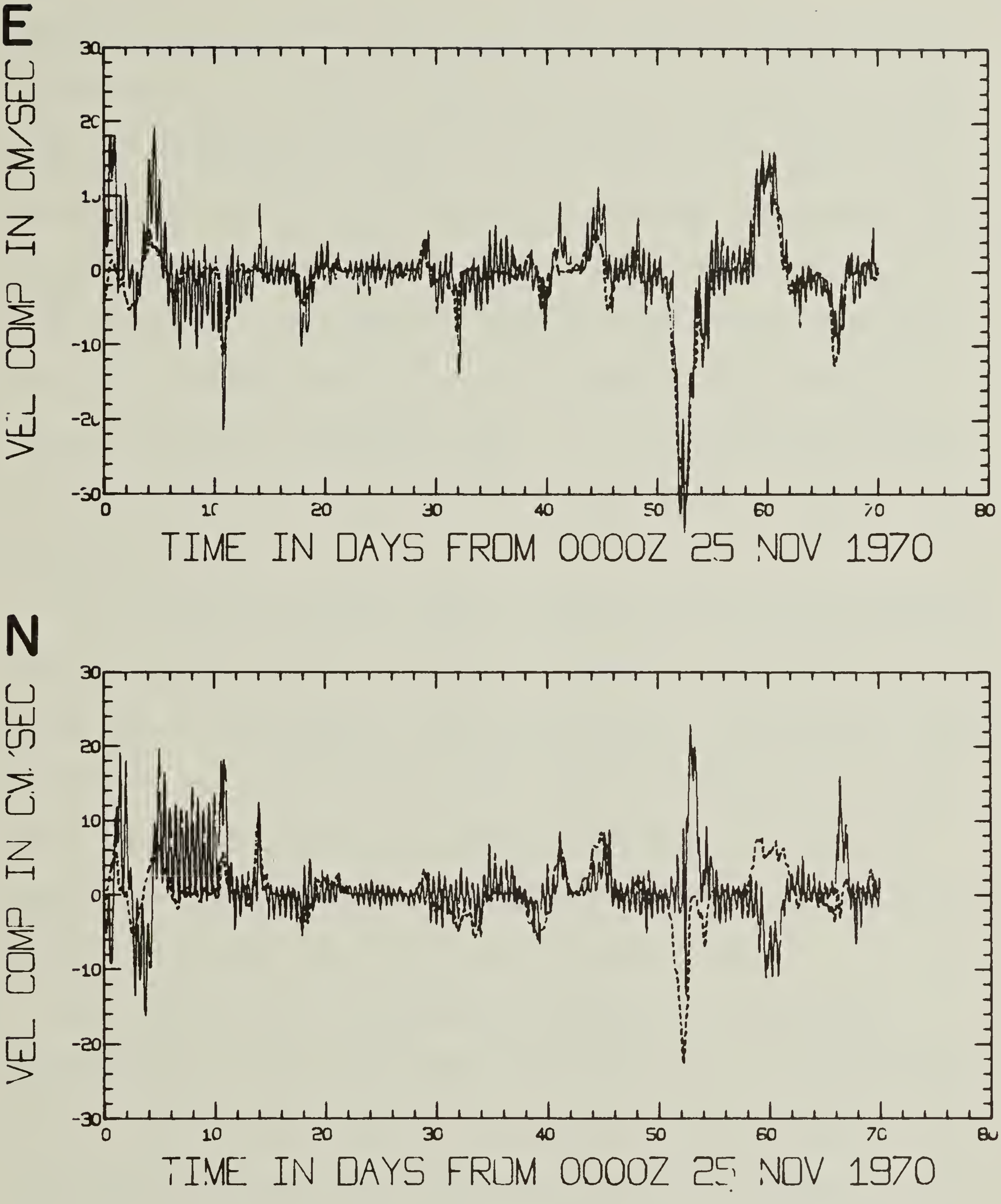

Fig. 14. Same as figure 13, but for 70m current meter on Mast C.

polated for intervals when the speed fell below the Savonious rotor threshold speed of 1 cm/sec. Since the records contain information about all frequencies from zero to 30 cycles per hour (cph), it is convenient to discuss them in terms of two arbitrary frequency ranges: a high frequency range of one to thirty cph, and a low frequency range of zero to 1 cph. The low frequency range will be discussed first. The current meter records were passed through a low-pass filter to eliminate frequencies above 1 cph. The resulting records for site C, 40m and 70m depths (C40, C70) are shown in figures 13 and 14 respectively.

The records C40 and C70 shown in figures 13 and 14 give relative currents (relative to the drifting ice station). Also plotted on the same figure is the negative of the ice velocity. The negative of the ice velocity has been plotted to show what the current meters would have recorded, if they had been dragged through still water. In figures 13 and 14 the absolute current may be seen as the departure of the relative current curve from the ice velocity curve.

The current meter records at 40m (figure 13) are generally characterized by large sinusoidal oscillations with a constant period of about twelve hours, plus more random low frequency behavior. The sinusoidal oscillations are only prevalent near the beginning of the record. The current meter records at 70m (figure 14) are characterized by persistent sinusoidal oscillations modulated by lower frequencies. In a later section these strikingly uniform sinusoidal oscillations will be shown to be inertial motions. The ubiquity of inertial motion in the ocean has only very recently come to be realized.

Inertial current motion is a solution to the simple linearized

equations of fluid motion in a rotating system such as the earth. By including only the mass-acceleration and Coriolis terms, the equations have a form

$$\begin{aligned} \frac{\partial u}{\partial t} - fv &= 0 \\ \frac{\partial v}{\partial t} + fu &= 0 \end{aligned} \qquad (1)$$

which is satisfied by

$$\begin{aligned} u &= A \sin ft \\ v &= A \cos ft \end{aligned} \qquad (2)$$

where (u,v) are the two components of fluid velocity, and f is the Coriolis parameter. On the earth, f depends on the latitude φ, following

$$f = 2\Omega \sin\varphi \qquad (3)$$

where Ω = magnitude of the earth's angular velocity vector.

Note that the (u,v) solution is a circular rotating vector, rotating clockwise with a frequency, f, usually referred to as the inertial frequency. At T-3's latitude of $85^{\circ}30'$ N, the inertial frequency corresponds to a period of 12.001 hours, which is just what is observed in the oscillations of figures 13 and 14. The inertial motion characteristics will be examined later in more detail. First, the transient currents with frequencies lower than the inertial frequency will be examined.

There are major differences between the current behavior at 40m in the upper mixed layer (figure 13) and at 70m in the continuously stratified layer below it (figure 14). With the exception of the first

ten days of the record, all currents at 40m damp out within a day or two after the ice cover has ceased moving. The uniform upper layer apparently cannot sustain a velocity shear. The inertial currents at 70m on the other hand show little sign of damping during intervals between ice motion events.

The exception of no damping occurring during the first ten days of data at 40m might be attributed to persistence through late autumn of some stratification just under the ice, a consequence of the presence of summer melt water. Hydrographic data collected through the year suggests this possibility.

To examine the lower frequency transient current, the current records shown in figures 13 and 14 were passed through a second low pass filter to eliminate frequencies at or above the inertial frequency. Figures 15 and 16 show the resulting mean currents, here converted from relative to absolute currents. The fixes from satellite navigation are placed on the same figure. There is a marked tendency for the ice motion to impart a steady current to the water, in the same direction as the ice movement. This tendency is not as clear for 40m as it is for 70m, because of the rapid damping in the upper homogeneous layer.

Examination of figure 16 shows some positive correlation between ice displacement d_{ice} and the mean current V_g at 70m depth, but for the north component of motion only. The peculiarly different nature of the first ten days of the record, due to persistence of summer stratification of the upper layer, also shows up in figure 16. The mean current and ice displacement show marked negative correlation during these ten days.

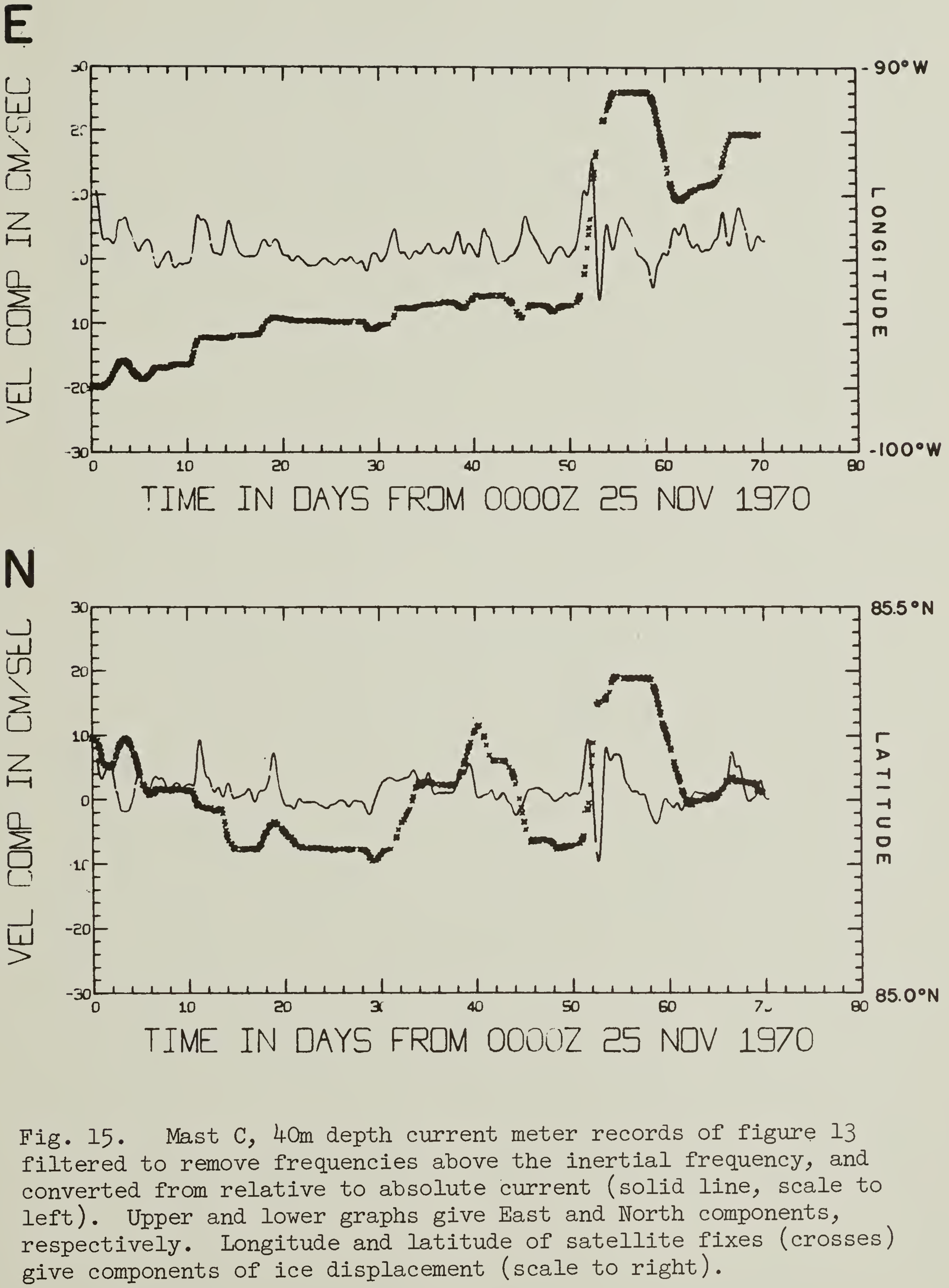

Fig. 15. Mast C, 40m depth current meter records of figure 13 filtered to remove frequencies above the inertial frequency, and converted from relative to absolute current (solid line, scale to left). Upper and lower graphs give East and North components, respectively. Longitude and latitude of satellite fixes (crosses) give components of ice displacement (scale to right).

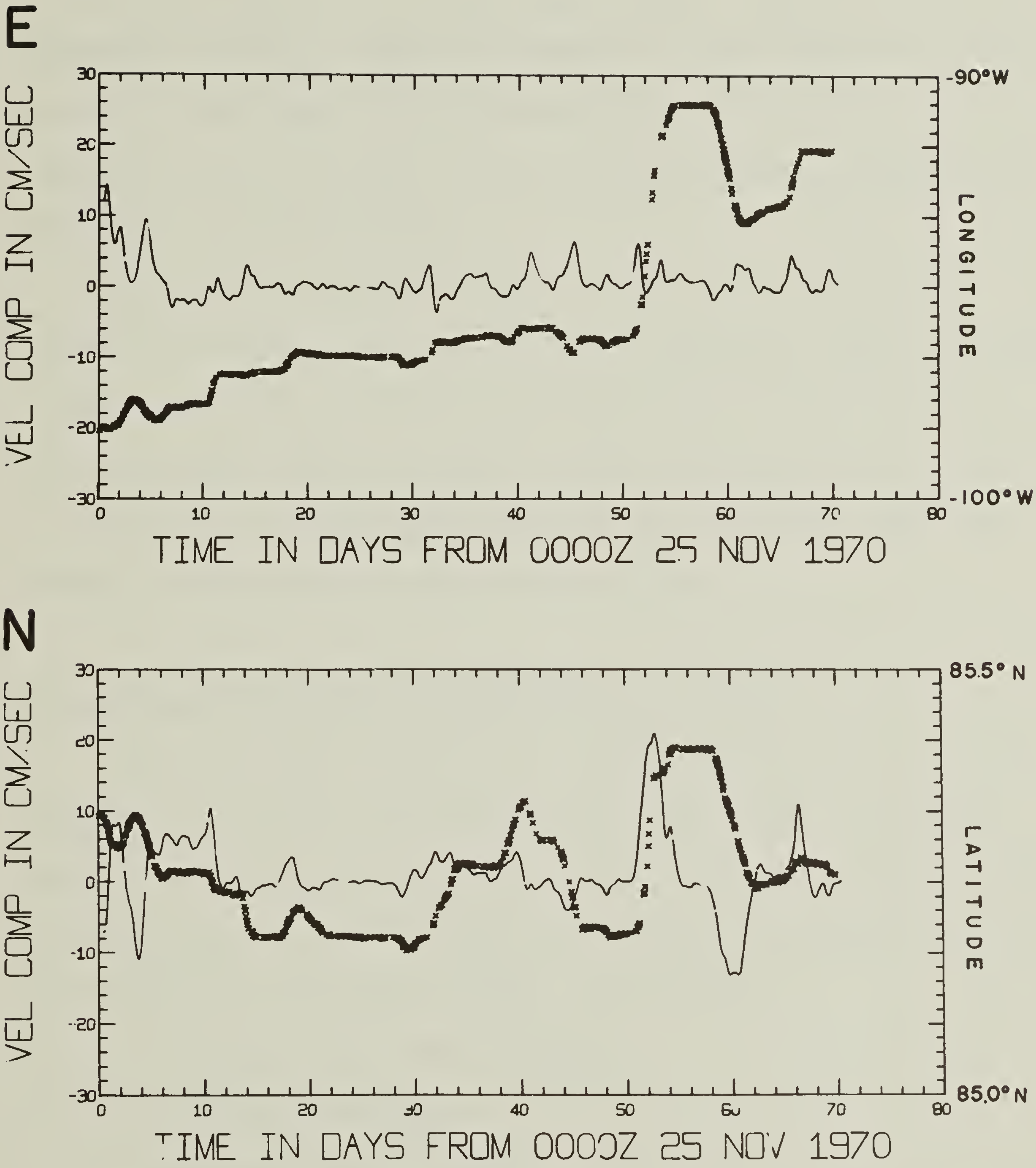

Fig. 16. As in figure 15, but for Mast C, 70m depth current meter.

No clear correlation between d_{ice} and v_g is evident in the east component of motion. Especially lacking is an east component current response to the large ice displacements of days 52 and 59. The reason for this will become clearer in other graphic presentations of the data to be given shortly.

Figure 16 also shows that any ice displacement, and any mean current over a period of a month or two was the vector sum of transient currents induced by a few discrete displacements of the ice cover. These transient currents can move in any direction, and the addition of one or two ice displacement events to any given month would have changed the monthly mean current significantly.

Other Methods for Graphical Presentation of Currents

There are always difficulties in graphic presentation of vectors measured at different points in space and time. There are various methods, and each has its own merits. The component plot has already been presented. It tends to emphasize the high frequencies over the low frequencies. The other methods to be used are:

1. The progressive vector diagram
2. The vector track plot
3. Spectrum analysis results

Each of these three graphical methods, and the features it best emphasizes will now be discussed in turn.

The Progressive Vector Diagram

In the progressive vector diagram, all the velocity vectors of a time series are placed head to tail, and the resulting displacement of

a particle carried by these currents is drawn out. Figure 17 gives the progressive vector displacement versus time for currents at 40m and 70m, and the drift track of T-3. The progressive vector diagram is made from absolute, not relative currents. Note that most of the displacements are associated with a very few major storms. The mean velocity associated with all three displacement vectors over the 70 day record is around 2cm/sec. The progressive vector diagram also shows, that to a very rough approximation the ice island and the mean currents, both at 40m and 70m, tend to travel together.

The area enclosed by figure 17 has been added as a detail to all other figures showing the whole Arctic region.

In figure 17 the surface wind vectors have been added to the ice island drift track. The vectors point in the direction toward which the wind blows. The ice nearly always moves to the right of the wind vector by some acute angle which is distributed around a peak at 30°, following Nansen's rule. This figure shows how high winds during storms correlate with rapid drift of the ice cover. All ice displacements shown in figures 15 and 16 were caused by storms.

One major trouble with progressive vector diagrams of currents measured with a current meter is that the point of observation is constantly changing relative to a particular water parcel. The progressive vector result is not the same as a Lagrangian tag on a particular parcel of water. With these considerations, figure 17 may be giving as good agreement as could be expected between a Lagrangian ice drift track and a semi-Eulerian derived current track.

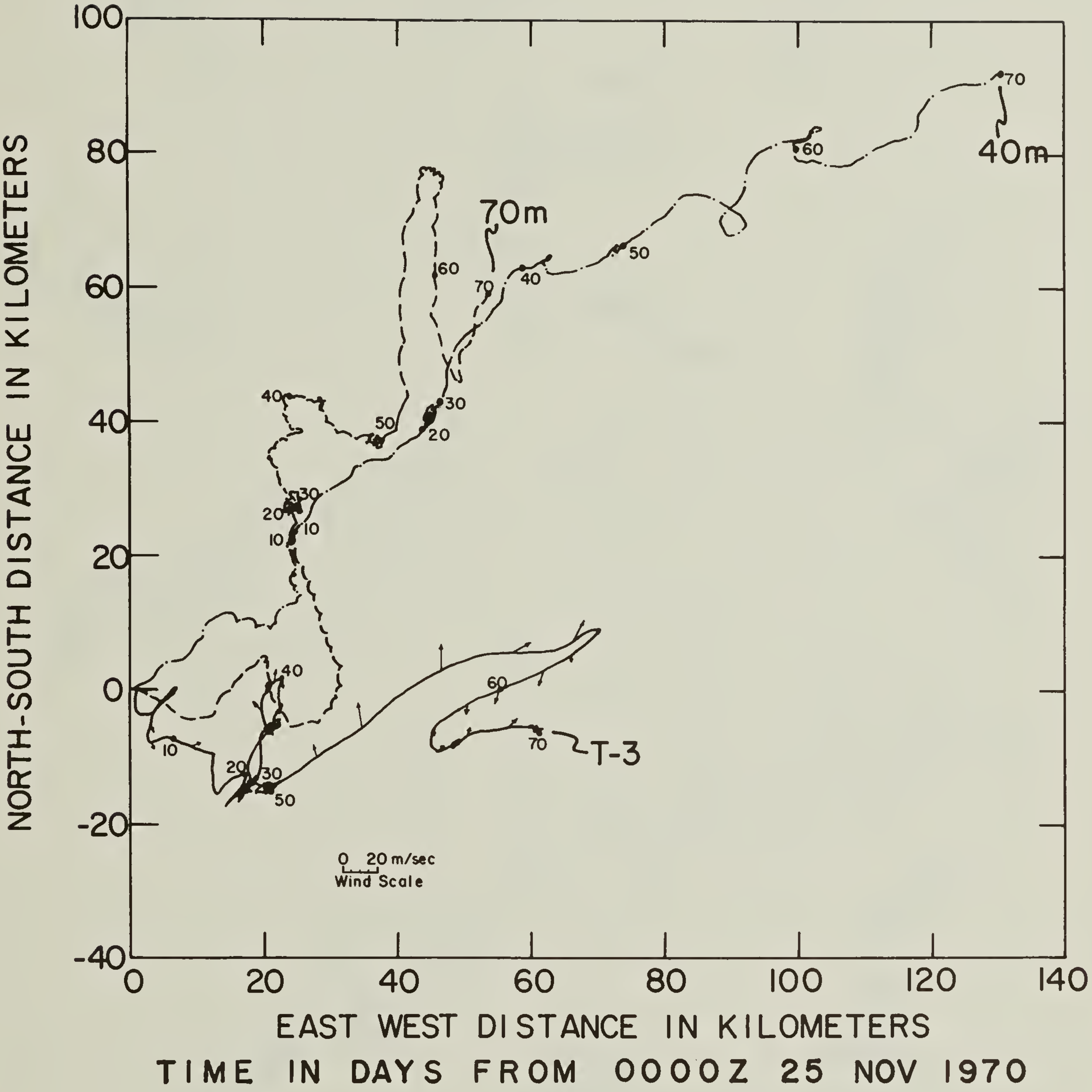

Fig. 17. Progressive vector diagram, giving 40m and 70m progressive vectors. T-3 drift track also shown, with wind vectors along the track, pointing in direction toward which wind blows. The area covered in this figure is given as an insert in other figures showing the whole Arctic region.

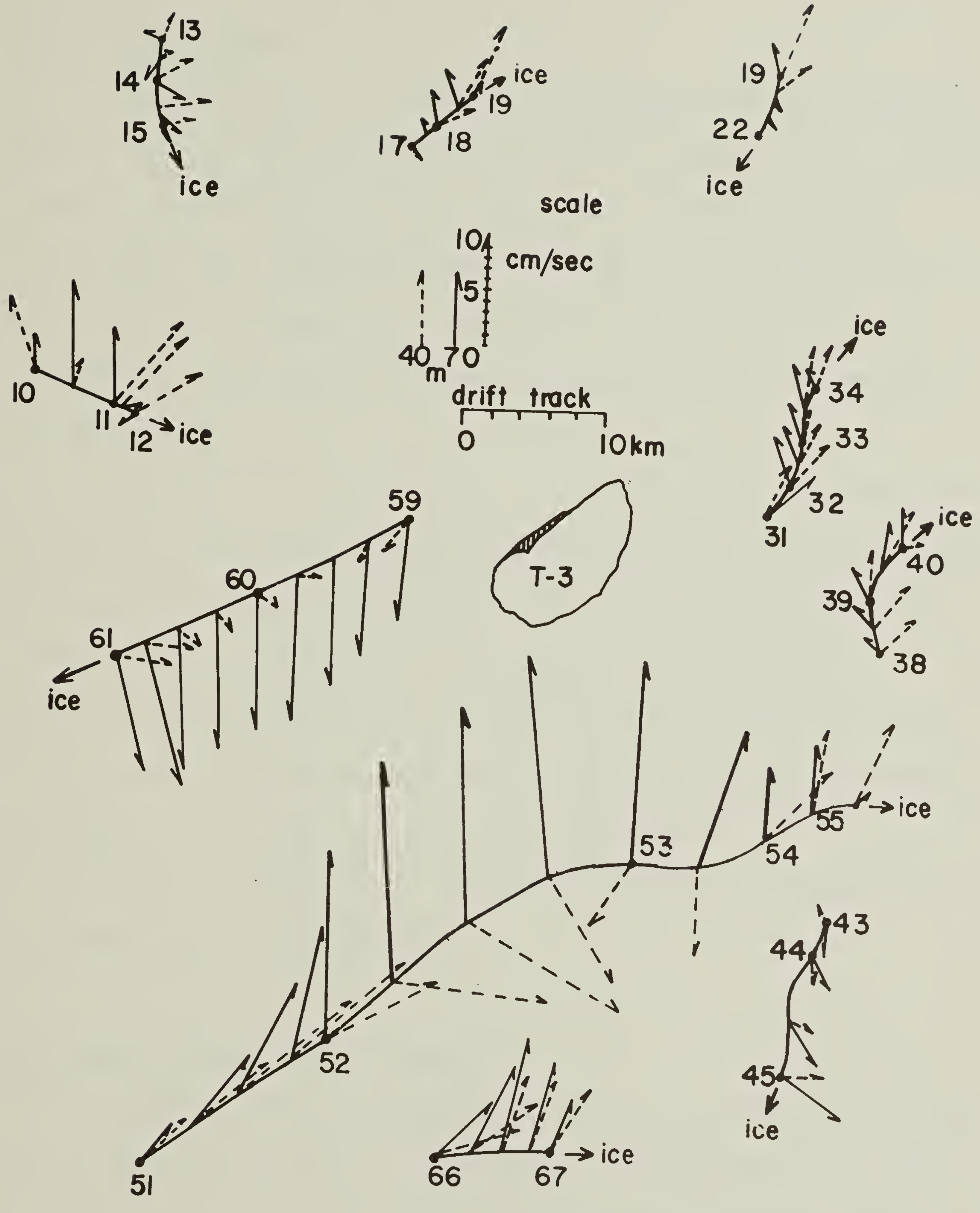

Fig. 18. Vector track diagram, giving segments of T-3's drift track. 40m and 70m low frequency transient absolute current vectors are placed along the track. Time marked in days from 0000Z 25 Nov 1970 along drift tracks. Outline of T-3 oriented as during experiment (North is to top of diagram), with Colby Bay (hatched lines). 70m flow always is to left of ice drift direction, while 40m flows either right or left.

Vector-Track Diagram

To examine better the low frequency transient current behavior, which is most prominent during periods of ice motion, there is another method of graphical presentation, which here will be called the vector-track plot. The daily mean of the absolute current vector is plotted with its origin at the appropriate position along the ice drift track. Both 40m and 70m mean current vectors are drawn along the drift track.

In figure 18, the vector track is shown for the major periods of rapid ice motion. The outline of T-3 is shown in the figure, properly oriented with respect to true north. The current vectors generally point forward in the direction of ice motion and to one side or another of the ice drift track. The 70m vector in almost every case points to the left of the drift track. The 40m vector points forward, but either to the right or left of the drift track.

Further discussion of the low frequency transient currents will be reserved for a later chapter.

Spectrum and Cross Spectrum Analysis

One last method for presenting the data is by obtaining spectrum and cross spectrum results. The method of BLACKMAN and TUKEY (1958) is used. Because of the extremely large number of sampled points in any one of the current records (1/minute $\times$ 70 days $\cong$ 100,000 pts) it was desirable to obtain the spectrum in two parts: high frequency and low frequency.

The high frequency spectrum was obtained by choosing an interval of data about one day in length, at a time where little or no ice

motion was occurring (during 29-30 November 1970). The low frequency part was obtained by using the entire 70 day record of the experiment.

The data had to be "pre-whitened" by passing it through a differencing filter (JENKINS, 1968) before taking a spectrum. This cuts down the low frequency power of the inertial and lower frequencies which otherwise would completely contaminate the spectrum. The resulting spectrum for C4ON is shown in figure 19 after the gain of the difference filter has been divided out of the raw spectrum.

The spectrum for C4ON in figure 19, as well as all subsequent spectral estimations, were performed with 20 degrees of freedom. Tables 2a, b, c, from GRANGER (1964) are used to find the 95% confidence limits.

To handle the low frequency spectral analysis, the low-pass filtered records, which were subsampled every 1/2 hour were used (figures 13 and 14). The records were converted to absolute currents before calculating spectrums. Care must be taken to divide out the gain of the low pass filter, and to similarly correct the spectrum for the effect of this and any other filters applied to the raw data, before presenting a final, true spectrum. The 1/2 hour subsampled data was difference filtered for pre-whitening purposes for this low frequency analysis also.

The spectrum of record C4ON is given in figure 20, along with the high frequency tail of figure 19. The inertial peak stands out strongly in the spectrum against a background of energy falling off with a fairly uniform slope of around -5/3 or -2. There is also an increase of energy between 5 and 10 cph, including a peak at 10 cph which is not as significant as the inertial peak. This high frequency increase

TABLE 2a Power Spectrum Confidence Bands

Degrees of Freedom		Exceeded by P% of all Values			
	P	95%	90%	10%	5%
2		.05	.10	2.30	2.99
3		.12	.20	2.08	2.60
4		.18	.26	1.94	2.37
5		.23	.32	1.85	2.21
6		.27	.37	1.77	2.10
8		.34	.44	1.68	1.94
10		.39	.49	1.60	1.83
12		.43	.53	1.55	1.75
15		.48	.57	1.48	1.66
20		.54	.62	1.42	1.55
30		.62	.69	1.34	1.46
50		.69	.75	1.26	1.34
100		.77	.82	1.18	1.22

(From GRANGER, 1964)

TABLE 2b Coherence Confidence Levels

Degrees of freedom	8	12	16	20	24	32	40
median	.454	.361	.307	.272	.247	.212	.190
90%	.732	.607	.529	.475	.435	.377	.338
95%	.795	.672	.590	.532	.488	.425	.382

TABLE 2c Confidence Bands for Phase Angle, in Degrees

95% ± confidence bands
Coherence

Degrees of freedom	.1	.2	.3	.4	.5	.6	.7	.8	.9	.10
8	56	45	37	31	27	22	18	14	4	0
12	50	39	31	26	22	18	15	11	3	0
16	46	35	27	23	19	16	12	10	3	0
20	43	32	26	21	17	14	11	9	2	0
24	41	30	23	19	16	13	10	8	2	0
32	36	26	20	17	14	11	9	7	2	0
40	33	23	18	15	12	10	8	6	2	0

(From GRANGER, 1964)

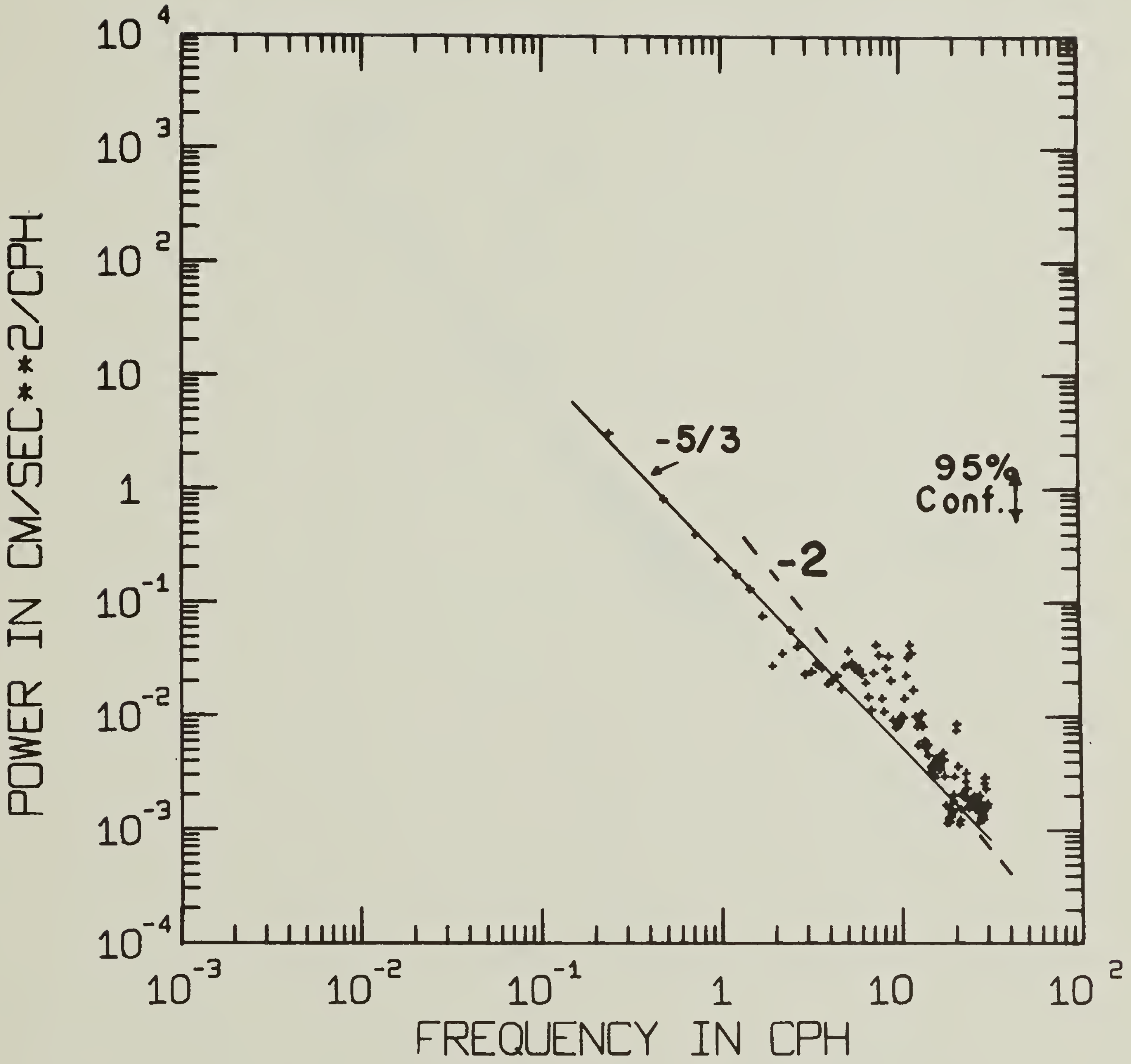

Fig. 19. High frequency spectrum, for 40m current. Spectrum obtained from one-minute sampled data for 29-30 Nov 1970, with 20 degrees of freedom. Arrows give 95% confidence limits. A -5/3 slope is drawn on this log-log diagram.

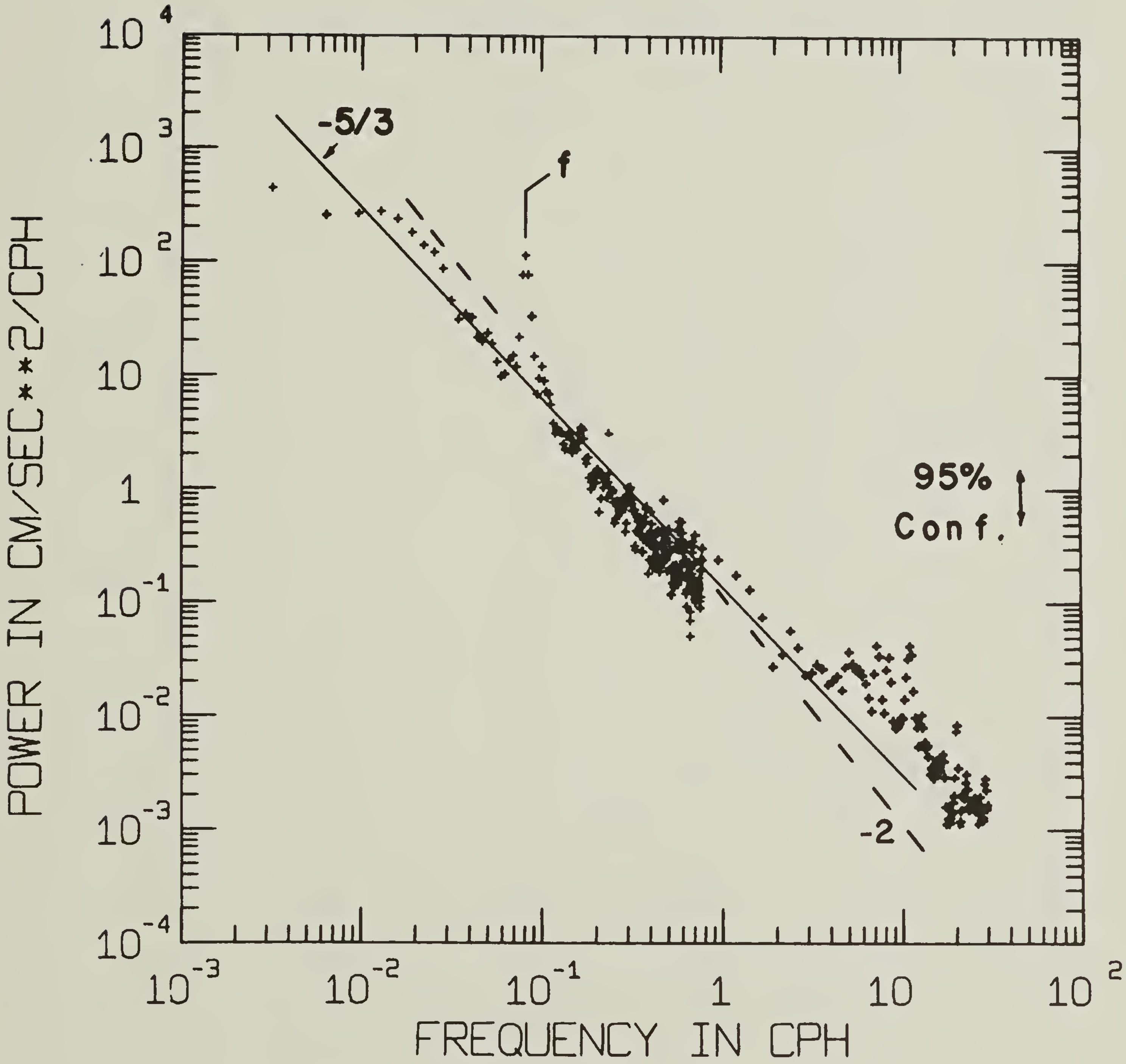

Fig. 20. Low-frequency spectrum for 40m current, including the high-frequency tail of figure 19. Spectrum based on entire 70 day record of absolute current. Degrees of freedom and confidence limits as in figure 19. Even fall-off of energy following -5/3 slope interrupted by energy peak at the 12 hour inertial frequency .

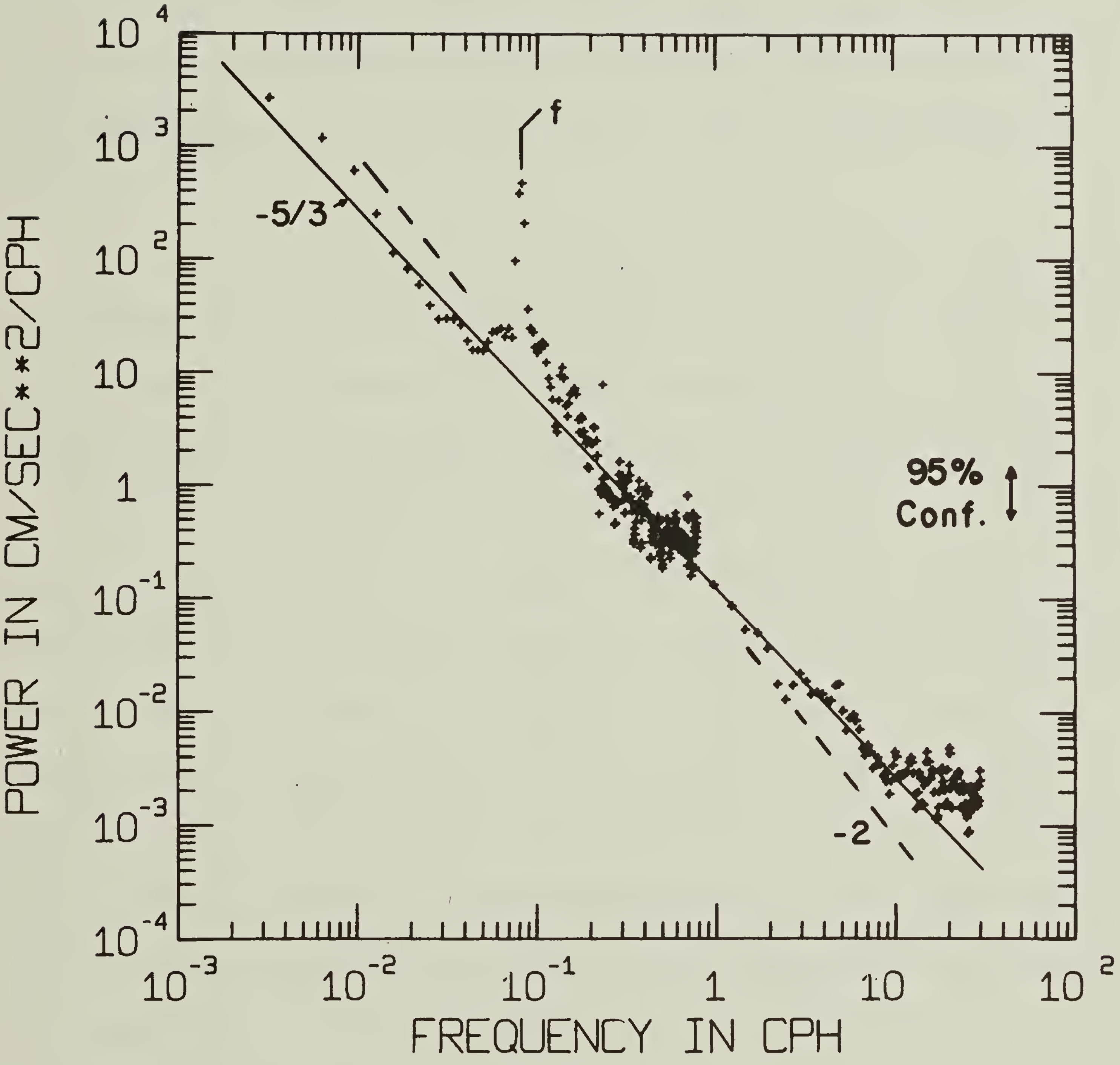

Fig. 21. Same as figure 20, but for 70m currents.

is associated with the local Vaisala frequency.

The power spectrum of record C70N is shown in figure 21. The spectrum shows the same even fall-off of energy as in the 40m record. It differs from the 40m record in having a more intense inertial peak, and in lacking any peak in energy around 10 cph. Both 40m and 70m spectrums appear to reach a noise level of $2x10^{-3}$ $(cm/sec)^2/cph$ at 20 cph.

There is some discontinuity in the spectrums where the high and low frequency parts join near 1 cph. This is especially true for the 40m spectrum. The reason why the 40m high frequency energy seems a little high is straightforward. During much of the time while the ice cover was not in motion, the current at 40m was zero. In selecting a one-day interval for the high frequency spectral estimation, a day with non-zero current was chosen, in order to obtain an interesting result. Thus the energy at 1 cph for this day is high in comparison with the average energy over the 70 day duration of the experiment. Since the 70m current did not go to zero like the 40m current during periods of no ice movement, the one day selected for the high frequency spectral analysis was typical of the average energy level at that depth.

The -5/3 or -2 slope of figures 20 and 21 on a log-log plot means that kinetic energy of the current follows a power law of frequency, with the exponent of the power law given by the measured slope. Similar results have been seen before in current meter records by other workers (WEBSTER, 1968), but the present results extend over a wider range of frequencies.

The -5/3 slope is highly suggestive of an energy-dissipating cascade from larger to smaller scales of motion, following the theory

of KOLMOGOROFF (1941) for homogeneous turbulence. The energy sources for such a cascade may be the low frequency large scale synoptic weather patterns, and the inertial motion. A -2 slope would also nearly fit the observed spectrums, and various theories have been advanced predicting this slope. For example, PHILLIPS (1971) obtains a -2 law for any current meter moving through an undulating well-layered medium, with fluctuations only a result of the meter occasionally passing from the steady flow regime of one layer into the steady flow of another layer. K. BRYAN (personal communication) has shown that a field of internal waves at their limiting slopes also would show a -2 energy law. The data seem to favor slightly the -5/3 law.

The interpretation of the even fall-off of energy with frequency has yet to be settled. The spectrums of figures 20 and 21 are offered as additional evidence for future theoretical considerations. The spectrums have two important points already mentioned. The high frequencies are not affected by buoy or surface wave action, and the low frequency motion of the ice and water tend to go together, so that the current meter tends to follow the same water mass while under the influence of synoptic weather patterns. This would not be true for measurements made at a bottom-anchored current meter system.

There are a number of cross-spectral estimates of special interest. In what follows the squared definition of coherence is used, with

$$\mathrm{Coh} = \frac{(\mathrm{Co})^2 + (\mathrm{Quad})^2}{S_1 \cdot S_2} \quad , \quad \mathrm{Phase} = \tan^{-1}\left(\frac{\mathrm{Quad}}{\mathrm{Co}}\right)$$

where S_1 and S_2 are the autospectrums of the two series, and Co and $Quad$ are the Co- and Quadrature spectrums of the two series. In the various phase diagrams for pairs of time series, positive phase means the first series of the pair leads the second, while negative phase means it lags. The possible error in the phase is directly related to the associated level of coherence, and may be obtained from Table 2c.

The power spectrum of both the east and north components of C40 show almost exactly the same power at the inertial peak. The cross-spectrum of the two components (figure 22) shows little significant coherence except around the inertial frequency. There, coherence approaches 0.8 with associated phase of east lagging north by $97^\circ \pm 9^\circ$. One would expect a 90° phase difference between components for a circularly rotating vector moving clockwise. The cross spectrum of the two components of record C70 (figure 23) gives a similar picture, with coherence of 0.9 and phase lag of $96^\circ \pm 2^\circ$, at the inertial frequency.

Other cross-spectrums of interest include the pairs C70N-C40N, A40N-C40N, A70N-C70N. There is no significant coherence between 70m and 40m (figure 24) except at the inertial frequency, where it reaches .65, with 70m lagging 40m by $60^\circ \pm 13^\circ$. This is in marked contrast with the high coherence and zero phase lag for the pairs at the same depths (figures 25 and 26). Coherence remains high for frequencies up to and beyond the inertial frequency, dropping below the significant level at .2 cph (corresponding to a period of 5 hours).

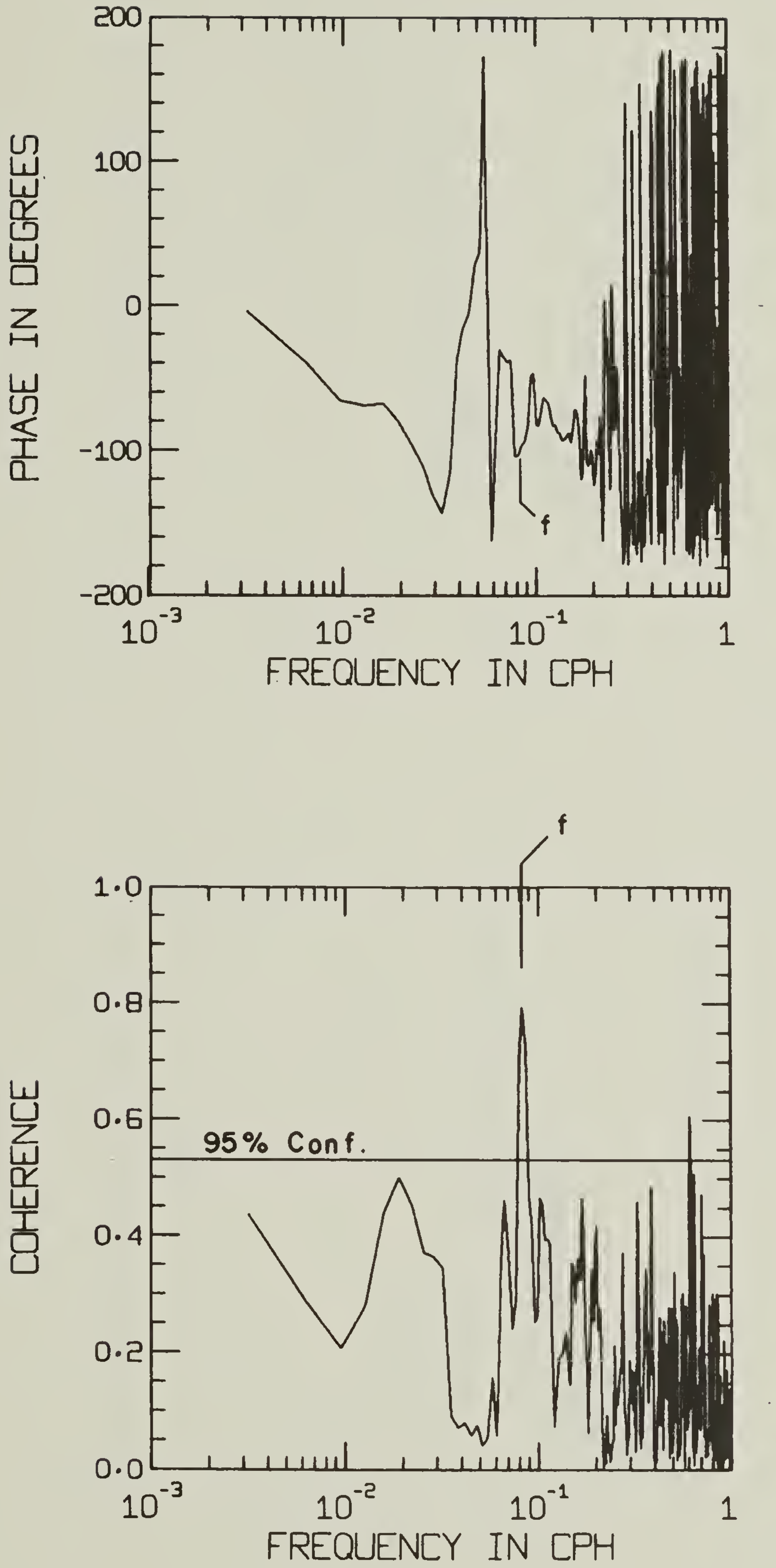

Fig. 22. Phase and coherence diagrams for cross-spectrum of East and North Components of 40m current, obtained from entire 70 day record of absolute current. 95% confidence level for coherence is indicated.

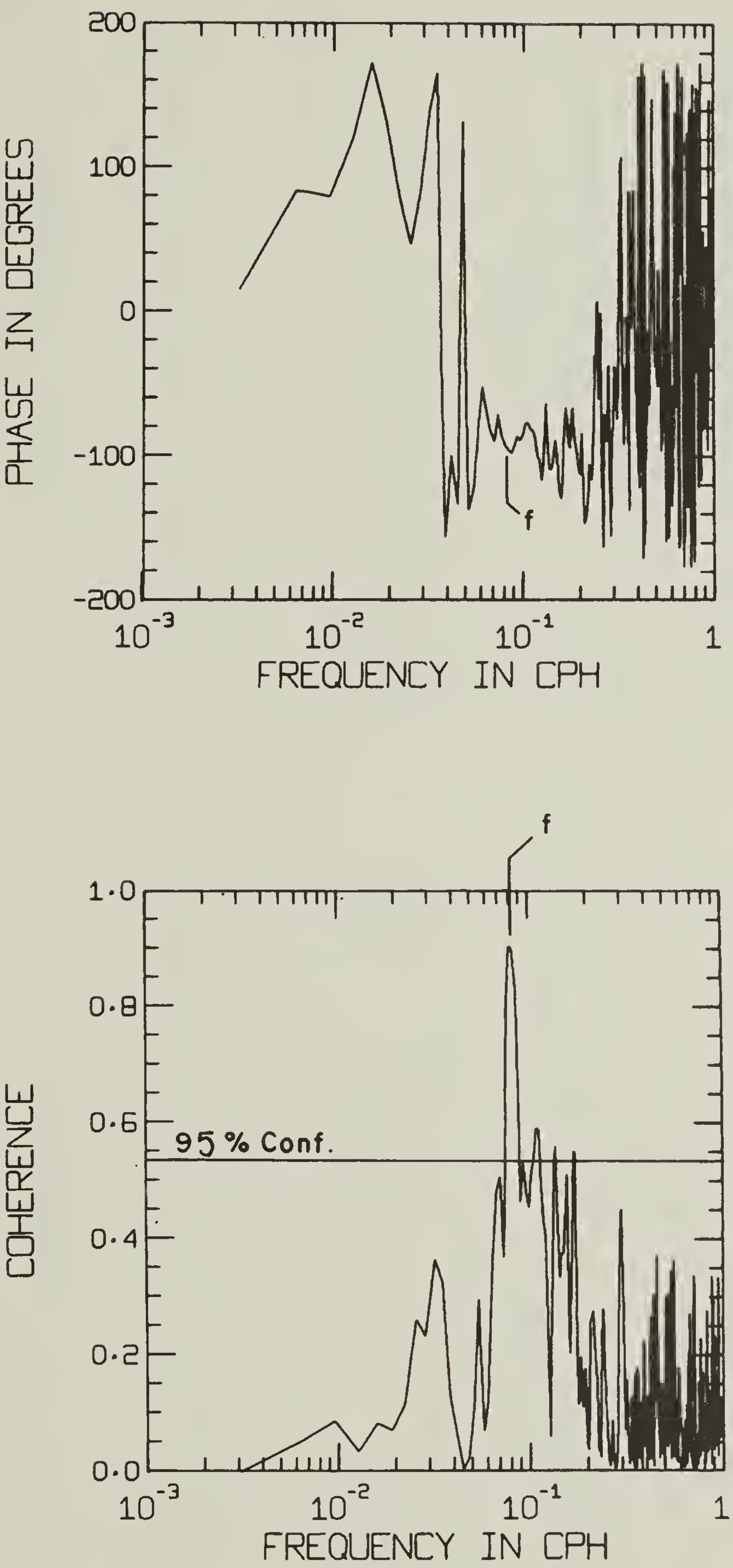

Fig. 23. Same as figure 22, but for 70m currents.

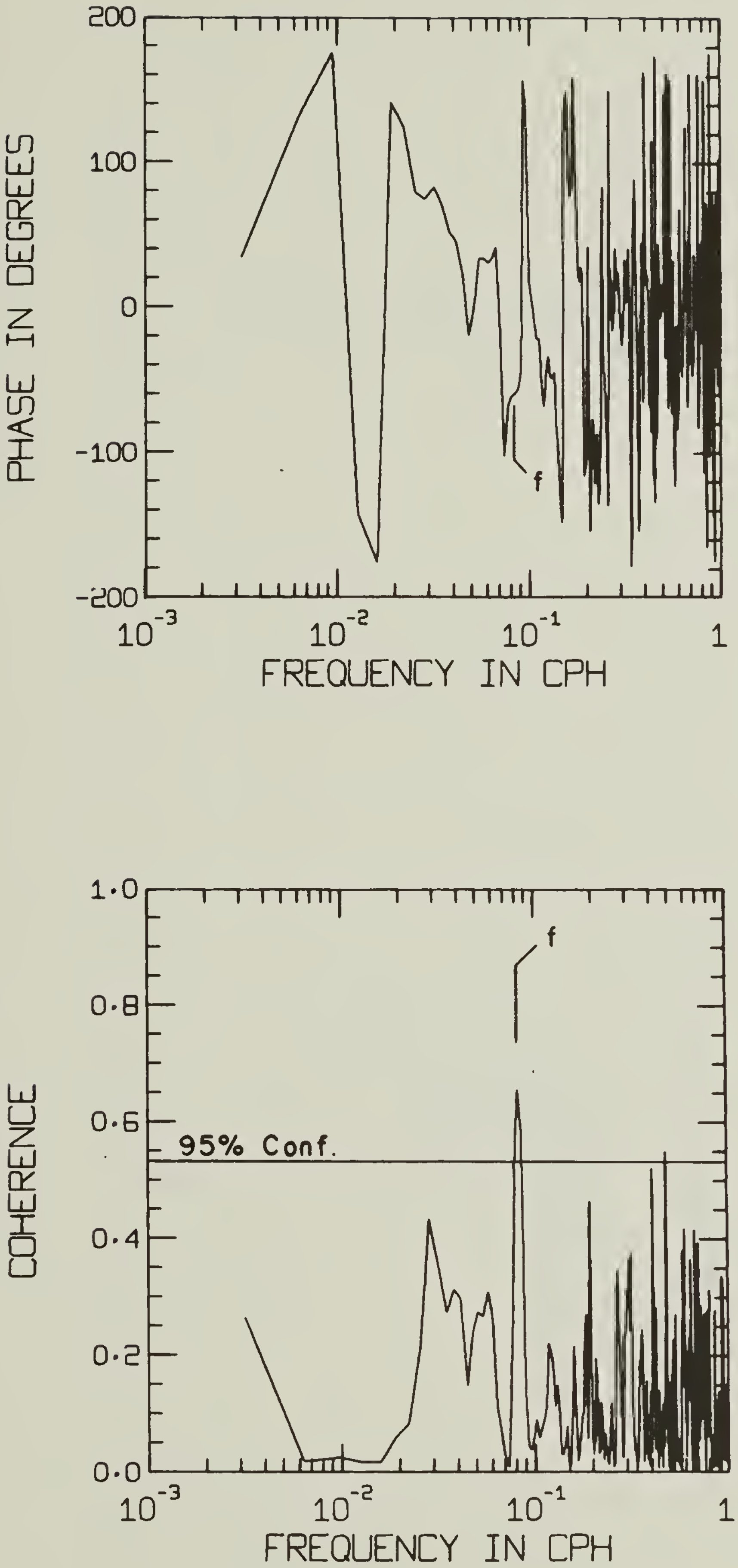

Fig. 24. Cross-spectrum results between north components of 70m and 40m currents measured at Mast C. Only significant coherence occurs at the inertial frequency f .

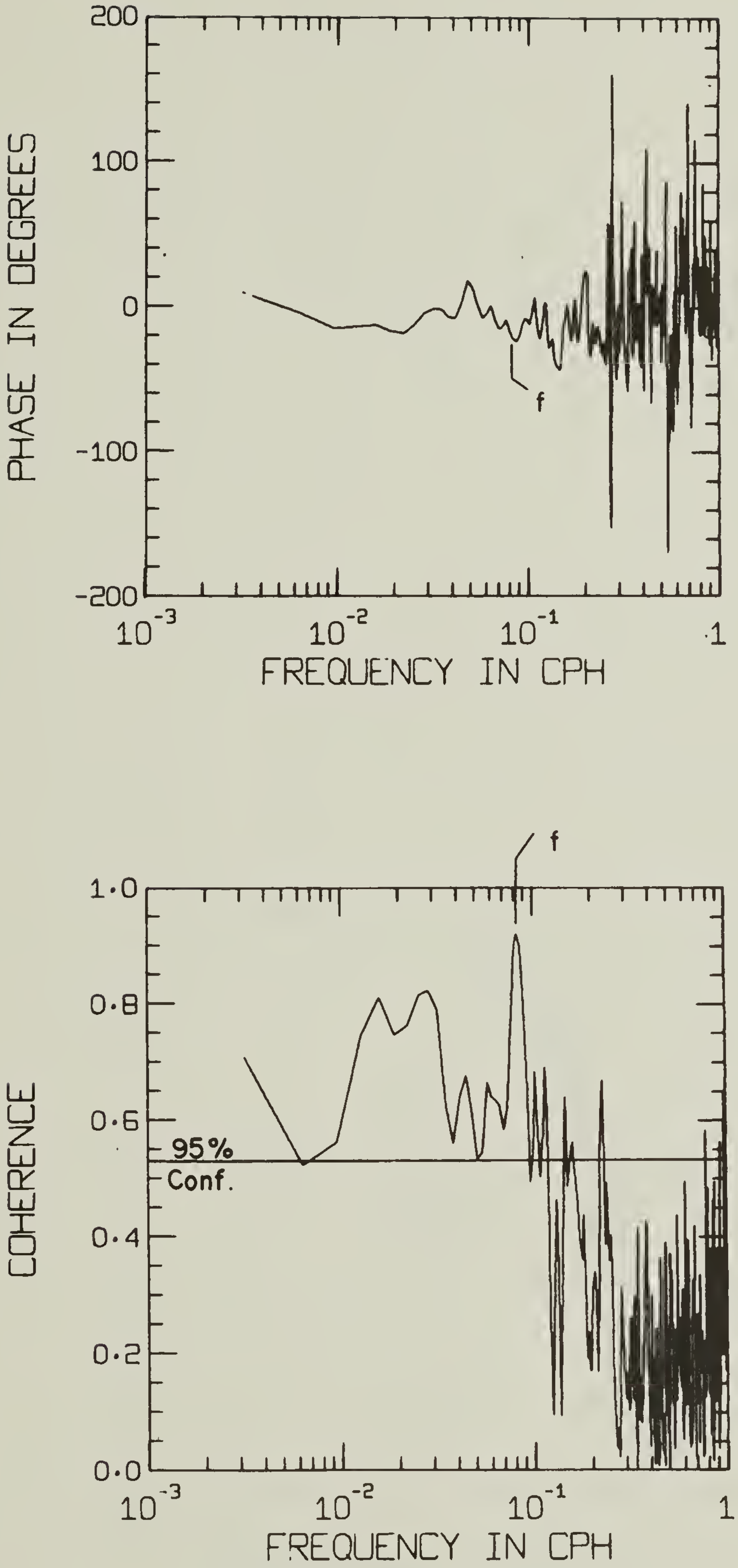

Fig. 25. Same as figure 24, but for currents measured at 40m from Mast A and at 40m from Mast C. Horizontal separation between masts is 370m. Significant coherence up to .2 cph (5 hour period).

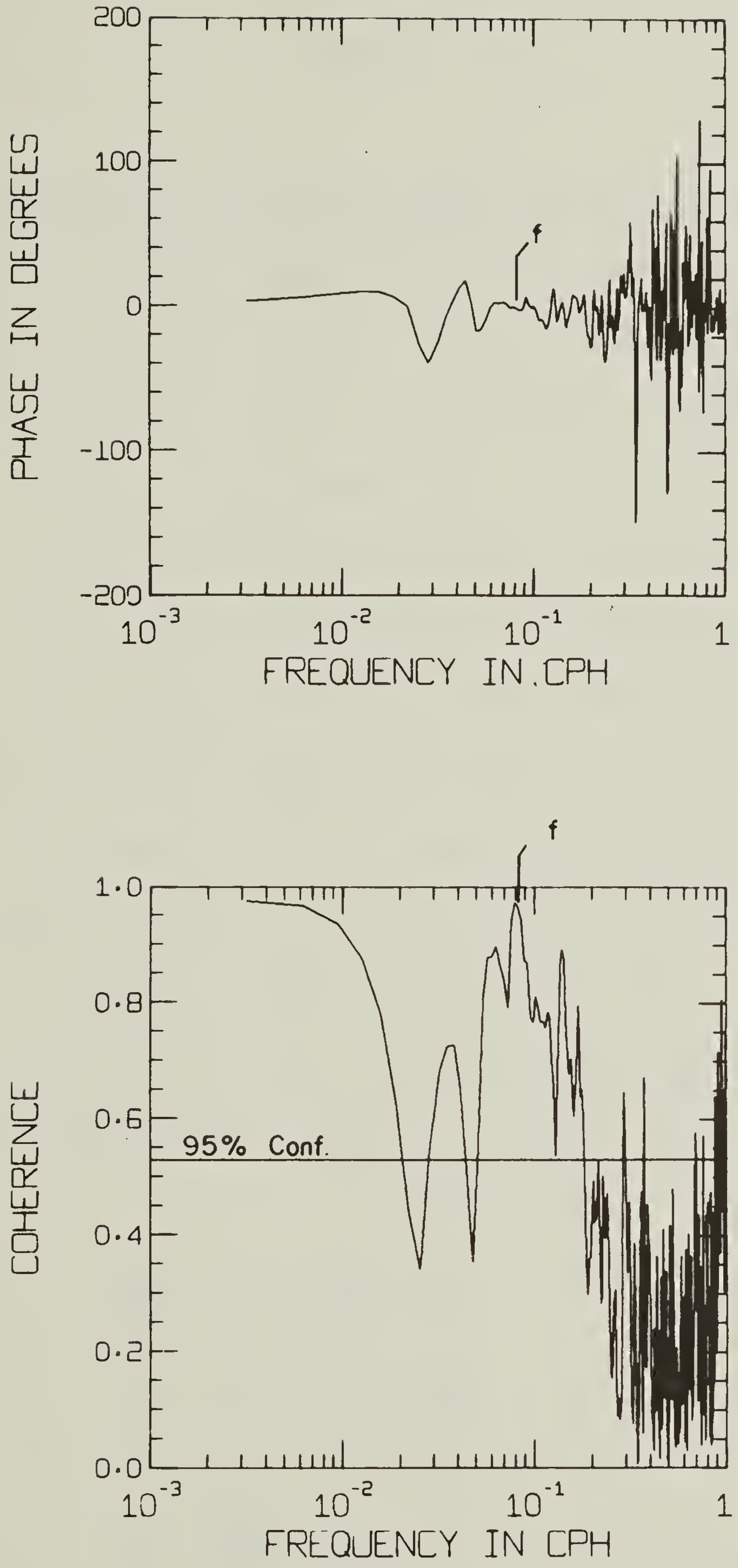

Fig. 26. Same as figure 25, but for currents measured at the 70m level at Masts A and C. Significant coherence up to .2 cph.

THEORY

The Pollard Theory of Geostrophic and Inertial Currents

POLLARD (1970) has summarized contributions to the theory of inertial and geostrophic current theory by ROSSBY (1937), STOMMEL and VERONIS (1956) and others. He presented a model including effects of Coriolis force, pressure gradients, and density stratification. To model the driving stress at the surface, due in his case to the wind, and in the Arctic due to ice movement, he considered that momentum injected into the ocean by stress at the surface is rapidly and evenly distributed through the upper mixed layer by mixing processes. For a valid model the time for this mixing must be short compared with the inertial period. The surface stress is then replaced by a body force distributed equally through the upper mixed layer.

Pollard begins with the linearized fluid equations of motion and continuity, which take the form

$$\begin{aligned} &\frac{\partial u}{\partial t} - fv + \frac{\partial p}{\partial x} = 0 \\ &\frac{\partial v}{\partial t} + fu = \frac{1}{\rho}\tau Z(z) \\ &b + \frac{\partial p}{\partial z} = 0 \\ &\frac{\partial b}{\partial t} - N^2(z)\, w = 0 \\ &\frac{\partial u}{\partial x} + \frac{\partial v}{\partial y} = 0 \end{aligned} \qquad (5)$$

where u and v are velocities in the x and y directions, w is vertical velocity, b is the buoyancy acceleration $\rho' g/\bar{\rho}$ where density $\rho = \bar{\rho} + \rho'(x,z,t)$ and $N(z)$ is the Brunt-Vaisala frequency defined by $N^2(z) = (g/\bar{\rho})\, \partial \rho'/\partial z$. f is the Coriolis parameter. τ is the body force equivalent stress, and $\mathcal{Z}(z)$ is its distribution with depth.

A solution to these equations may be obtained by the method of normal modes. One solution by Pollard (his case II), was for a strongly stratified layer of thickness H_1 overlying a weakly stratified bottom layer of thickness H_2. This solution (Equations 6,7,8) can be separated into oscillatory and non-oscillatory parts. The non-oscillating part represents the geostrophic or mean current contribution. The oscillating part has eigen frequencies s_r which all lie within a few percent of the inertial frequency f for a wide range of typical ocean parameters.

non-osc.
$$v_G = [t]\frac{\tau}{\bar{\rho}} \sin kx \left[\mathcal{Z}_0 \phi_0'(z) + \sum_{r=1}^{\infty} \left(1 - f^2/s_r^2\right) \mathcal{Z}_r \phi_r'(z) \right] \tag{6}$$

osc.
$$\begin{cases} u_I = \dfrac{\tau}{\bar{\rho}} \sin kx \displaystyle\sum_{r=1}^{\infty} f/s_r^2\, \mathcal{Z}_r \phi_r'(z) \left\{ \cos s_r(t-[t]) - \cos s_r t \right\} & (7) \\ v_I = \dfrac{\tau}{\bar{\rho}} \sin kx \displaystyle\sum_{r=1}^{\infty} f^2/s_r^3\, \mathcal{Z}_r \phi_r'(z) \left\{ \sin s_r t - \sin s_r(t-[t]) \right\} & (8) \end{cases}$$

where $[t] = \begin{cases} t, & t<T \\ T, & t>T \end{cases}$, T is duration of stress, $s_r = f\left(1 + \dfrac{k^2}{f^2 \lambda_r^2}\right)^{\frac{1}{2}}$,

with $k = \dfrac{2\pi}{L}$, horiz. scale of stress, $\lambda_r = \dfrac{r\pi}{2 N_1 H_1}$, N_1=upper layer Vaisala freq.

Eigenfunctions $\phi_r'(z) = \begin{cases} \cos \dfrac{r\pi z}{2H_1}, & 0<z<H_1 \\ \cos\dfrac{r\pi}{2} \cos \dfrac{r\pi(z-H_1)}{2H_2} - \dfrac{H_1}{H_2} \sin\dfrac{r\pi}{2} \sin \dfrac{r\pi(z-H_1)}{2H_2}, & H_1<z<H_1+H_2 \end{cases}$

$\mathcal{Z}_r$ is the expansion of $\mathcal{Z}(z)$ in terms of eigenfunctions $\phi_r'(z)$.

Solutions were calculated from the Equations by digital computer, and checked by reproducing several of Pollard's figures. The solution's general characteristics are sketched as follows for a stress

$$\tau_x = 0 \quad \text{for all } t$$
$$\tau_y = \begin{cases} \tau_0 \text{ (constant)}, & t = 0 \text{ to } t = T \\ 0 & \text{otherwise} \end{cases} \qquad (9)$$

In a hodograph plot of the two velocity components, the non-oscillating part of the solution steadily increases while the stress is applied (figure 27a). During this time the oscillating part of the solution (u_I, v_I) follows the circle A for currents in the upper mixed layer, and circle B for currents below the upper mixed layer, as shown in figure 27a. The oscillatory part of the solution reaches a maximum velocity for times $t \cong \frac{1}{2}T_i, \frac{3}{2}T_i, \ldots$ where T_i is the inertial period, and goes to zero for $t \cong 0, T_i, 2T_i, \ldots$. Note that while the stress is being applied, the oscillating part has a mean transverse flow associated with it. This flow is to the right of the stress direction in the upper mixed layer and to the left below it. This transverse flow tilts the isopycnal surfaces down to the right of the stress direction. This increasing tilt must then be associated with the steadily increasing (non-oscillatory) geostrophic current V_G , flowing in the direction of stress.

When the stress returns to zero, the non-oscillating part of the solution thereafter retains the value it had attained at the time T. The oscillating part of the solution changes to follow a circle C centered on the origin, with radius $r(t=T) = (u_I^2(t=T) + v_I^2(t=T))^{\frac{1}{2}}$ (figure 27c). The time to complete one orbit or circle C is close to but slightly less than one inertial period. Thus the mean transverse flow has disappeared along with the stress, but the isopycnals remain at their final tilt position, in balance geostrophically with a constant current V_G. For times $t>T$, the radius r of circle C changes slowly compared to the inertial period, and this change is dependent on the horizontal scale features of the previously applied stress field.

From inspection of figure 27b for times when stress is being applied, current vectors averaged over one or two inertial periods make an acute angle with the stress direction. For the solution in the upper mixed layer, the averaged current vector veers to the right of the stress direction, while below the upper mixed layer, the averaged current veers to the left of the stress direction. Qualitatively, this character of the solution may be compared with the results of the present experiment, exhibited in the vector-track diagram (figure 18).

Thus far, mainly the time dependency of the solution has been discussed. The vertical profile of the current depends on the stratification. For the two-stratified-layer model (Pollard's Case II) Pollard has provided vertical profiles for typical deep ocean parameters. The solutions give mostly barotropic geostrophic or mean current through the deeper layer, with the possibility of intensification upward through the upper layer. The inertial current part of the solution also has maximum amplitude in the upper mixed layer and

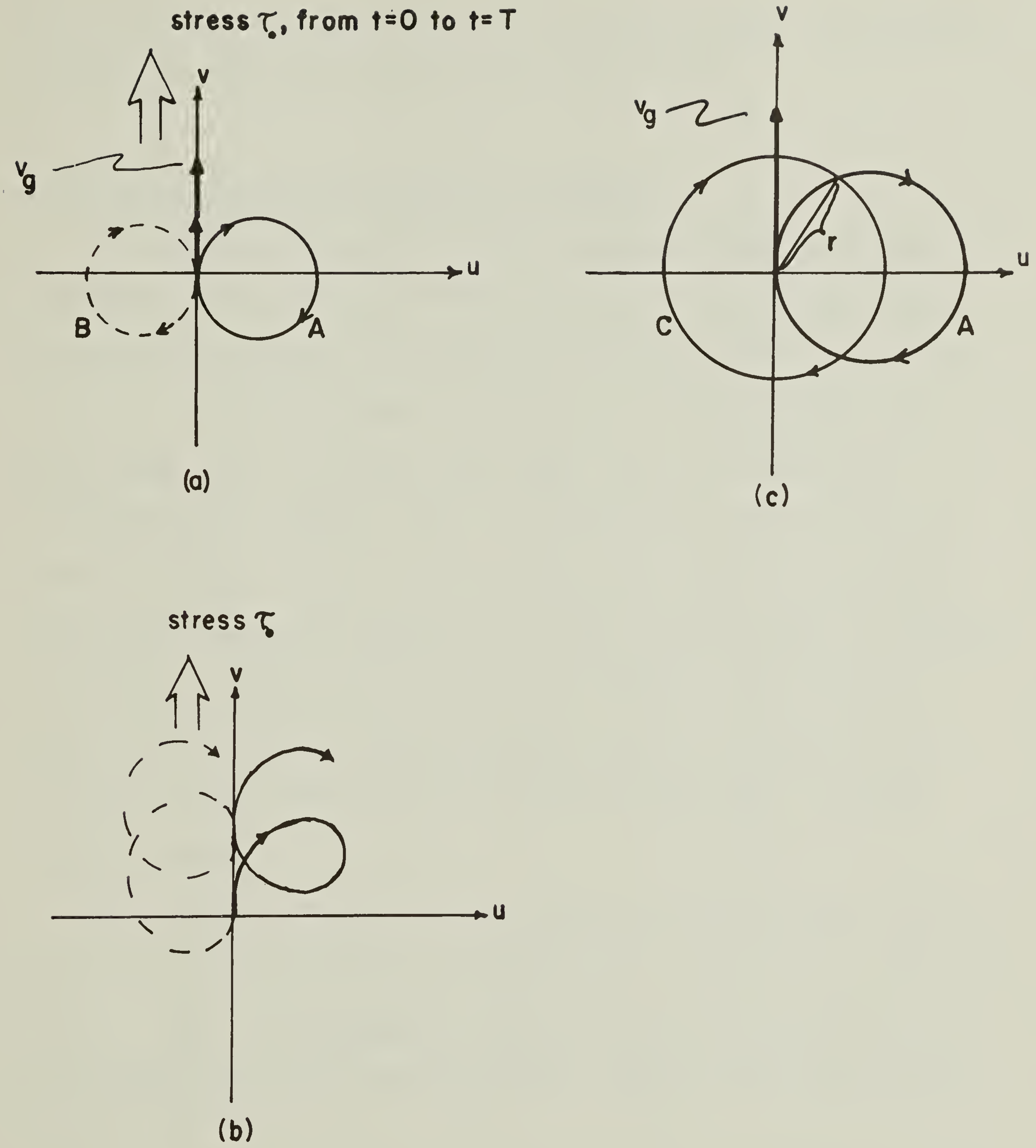

Fig. 27. Hodograph sketch of Pollard solution characteristics. (a) Stress turned on $t=0$ to $t=T$, geostrophic current v_g builds in the direction of stress, while inertially oscillating current (u_I, v_I) follows circles A (upper mixed layer) and B (below upper mixed layer). (b) Total current equals sum of v_g and (u_I, v_I), for upper mixed layer (solid line) and below upper mixed layer (dash line). (c) After stress turns off, geostrophic current remains constant, while inertial current switches from circle A to circle C.

just below it, decreasing rapidly with increasing depth. The inertial currents are very small throughout the lower layer.

Application of the Pollard Model to the Arctic

For the next step, parameters more typical of the Arctic were substituted. Water depth was taken as 1500m, upper and lower layer stratifications chosen corresponding to Vaisala periods of 14 and 70 minutes, with layer thicknesses of 250 and 125m respectively. An upper mixed layer was taken as the upper 50m of the 250m thick stratified layer. Surface stress is 1 dyne/cm^2. We are left to choose $k = 2\pi/L$, where L is the horizontal scale of the surface stress field, and also a position X in this field at which to calculate a solution. Kx will be taken such that $\sin(kx)=1$ for convenience. Figures 28a,b show the resulting vertical current profiles at time inertial periods, where stress was turned on from $t=0$ to $t=1.5$ inertial periods.

The vertical profiles of current from the solution show different results for k corresponding to horizontal ice stress scales of 125 and 500 km. There is no *a priori* reason to choose any particular k, but the smaller scale gives better agreement with profiling observations (figure 10).

Pollard's model for the wind stress over an open ocean requires an important modification for an ice-covered ocean. In the open ocean, when a storm has passed and excited currents in the upper mixed layer, these currents are free to continue. In an ice-covered ocean the ice usually stops moving before or shortly after passage of a storm. Currents created in a uniform upper mixed layer cannot sustain a

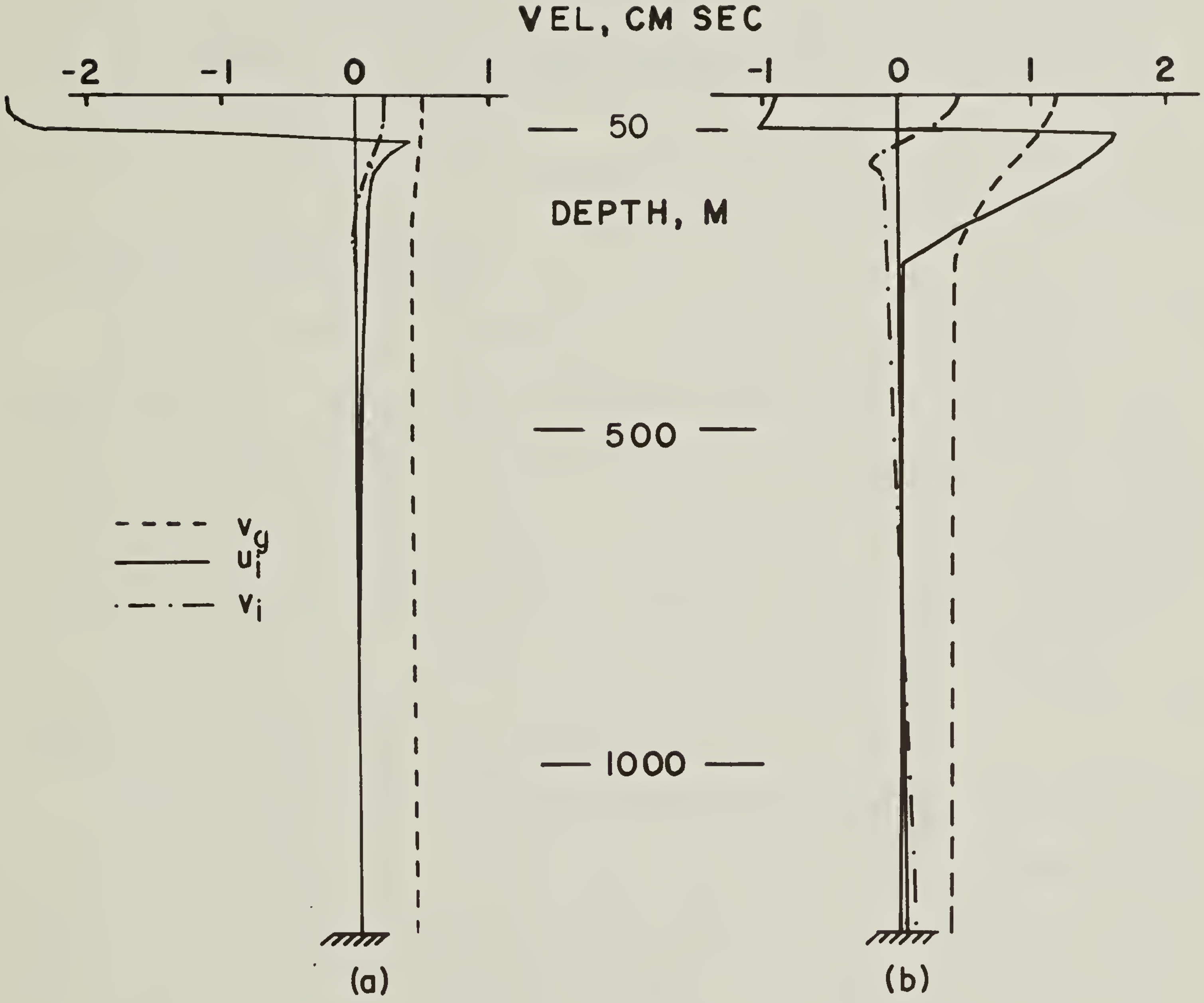

Fig. 28. Vertical profiles of currents for Pollard solution with typical Arctic parameters. (a) Horizontal scale of stress L = 500 km. (b) L = 125 km.

velocity shear with respect to this non-moving ice cover, and rapidly lose their energy. If this is the case, the current profiles of figure 28b would be slightly modified, with zero current above 50m, which is somewhat more in agreement with vertical current profile measurements, as in figure 10.

Validity of the Pollard Model

One basic physical assumption of the Pollard theory requires rapid mixing of stress through the upper mixed layer. The layer, because of its uniform density distribution, is not supposed to be able to sustain a mean velocity shear in the vertical. With the assumption of mixing on a time scale short with respect to the inertial period, the surface stress can then be replaced by a body force distributed through the entire upper mixed layer.

Evidence for rapid mixing comes from a Ross $100kh_z$ echo sounder record operated near the current meter array. The echo sounder often showed a strong return from planktonic organisms floating at the base of the upper mixed layer (HUNKINS, 1971), at a depth of 50m when these current measurements were made. The depth to the base of the upper mixed layer thus can be monitored continuously, with an accuracy of about 0.5m. Small undulations often occur, with amplitudes of about 1m, periods of a few minutes and longer. There are certain drawbacks in this sounder data. The organisms sometimes are not present so there is no return. At other times there are two or more returns separated by a few meters and it becomes difficult to follow any one return for more than a day.

Figures 29a, b, show the Ross record at 2 and 4 hours following

onset of an ice motion event. Figure 29a shows the interface fairly quiescent and still typical of times of no ice movement. Figure 29b, 4 hours after onset of ice movement, shows the beginning of vigorous motion at and above the 50m interface, with little disturbance below the interface. With this supporting evidence for rapid mixing, the Pollard theory will now be used as a framework for further discussion.

Fig. 29. Photographs of two one-hour segments of the Ross 100 khz echo sounder, 2 hours (upper photo) and 4 hours (lower photo) after onset of ice movement at 1100Z 5 Dec 1970. Base of 50m thick upper mixed layer clearly shows, with disturbances occurring in lower photo.

DISCUSSION OF TRANSIENT AND INERTIAL CURRENTS

Details of Transient Current Motion

It was previously stated that the mean (or geostrophic) absolute current and the ice displacement have a rough correspondence as shown in figures 15 and 16. The correlation of changes in mean current with ice displacement can be understood if

$$\Delta V_G \propto \tau_{ice} T \qquad (10)$$

where ΔV_G is the change in mean or geostrophic current, τ_{ice} is the stress exerted by the ice on the water, and T is duration of stress. Equation 10 is taken from POLLARD (1970), and is just a statement of Newton's second law of motion. It is convenient to assume that τ_{ice} is approximately proportional to ice velocity, V_{ice} although a V^2 law would probably be more physically accurate.

$$\tau_{ice} \propto V_{ice}. \qquad (11)$$

Then

$$\Delta V_G \propto V_{ice} T = d_{ice}$$

where d_{ice} is the ice displacement.

The vector track plot of the mean currents (figure 18) can be interpreted as showing the effect of Ekman transport to the right of the stress direction above the 50m interface, and to the left below the interface. The Ekman transport causes the isopycnals to tilt down 90° to the right of the ice displacement direction. This transport must be combined with the geostrophic current which builds up in the direction of ice stress, as the isopycnals begin to slope. Such a condition is shown in figure 27b. The result of these cross and

down stream transports would be a vector making some acute angle with the drift track. This angle would be to the right of the ice displacement direction for currents within the upper mixed layer, and to the left below this layer.

Ekman type transport has previously been observed from an ice floe by HUNKINS (1966). The ice floe had the same thickness as the surrounding pack ice, unlike the anomalous 30m draught of T-3. An Ekman spiral causing net transport to the right of the direction of ice movement was measured, with most of the transport confined to the top 18m of the upper mixed layer. Mean flow to the left at 70m would be the compensating current to satisfy conservation of mass under these conditions.

In the present experiment, during about half of the cases in the vector-track plots of figure 18, the 40m vector joins the 70m vector on the left side of the drift track. One possible explanation for this could be that these near surface measurements are being made too close to the draught of T-3, which disturbs them. This possibility may be checked by examining the 40m mean flow on the vector track plot, along with the orientation of T-3 during the experiment. When the ice island moves in such a way as to keep the current meters ahead of the island, one might expect the minimum effect of the island's draught. Inspection of figure 18 shows the current meters more at the "bow" of T-3 for intervals 17-19, 19-22, 31-34, 38-40, and more at the "stern" for intervals 10-12, 13-15, 43-45, 59-61, 66-67. The case 51-55 is marginally in between. Note that the first four cases have developed 40m flow to the right of the drift track, while the latter five have not.

A second possible explanation for the uncertain directional behavior of the 40m flow could be from the change in depth of the 50m interface following sloping of the isopycnals. The Ross echo sounder record showed that the interface came up to about 30m during the ice movement (10-12), and to about 41m for the movement (13-15). The vector track for these two cases shows the 40m current to the left in the former case, and indecisive in the latter case. A sufficiently shallow interface depth would put both current meters in the lower layer. The 70m instrument was twice as far from the interface as the 40m instrument. Therefore it is much less likely that isopycnal tilting could deepen the interface to 70m depth, and thus cause the 70m vector to point to the right of the drift track. This in fact was never observed to happen. The early termination of the Ross echo sounder record did not allow comparisons for later ice displacements.

The two abovementioned possible explanations suggested as giving the uncertain directional behavior of the 40m current vector also may explain why the 40m current magnitude is less than the 70m current magnitude.

From the observations shown in figures 15 and 16, it is actually more correct to say that the mean flow builds while the ice is moving, but when the ice halts, the mean flow rapidly drops back to zero. This decline in mean current occurs both at 40m and 70m. Since this decline in mean flow occurs at 70m, even though inertial currents constantly persist there, frictional dissipation cannot be invoked as the agent causing the disappearance of the mean (geostrophic) current. A frictional mechanism would erode both geostrophic and inertial motion. No acceptable explanation can presently be offered for under-

standing the flow situation following cessation of ice cover motion. The full internal wave equations may be involved, including effects of density stratification, Coriolis force, pressure gradients and viscous forces.

Synoptic Considerations of Transient Currents

The 0000Z daily surface pressure charts for the Northern Hemisphere produced by the U.S. Weather Bureau cover the area of the present experiment. For nearly every one of the 70 days of the experiment, the ice island drifted parallel to the pressure isobars, keeping higher pressures to the right of the drift track. This is in accord with the early work of ZUBOV (1945), referred to in the first chapter, and known as Zubov's rule.

The degree to which the ice island conforms to Zubov's rule is illustrated for the drift of days 38 to 40, best seen in the vector-track figure 18. The pressure charts for the three days are reproduced in figure 30. T-3's drift velocity is placed on the charts. There was negligible drift at the beginning of day 38, and the pressure chart shows very weak pressure gradients at T-3's position then. On days 39 and 40 a weak low moved by T-3 going toward the pole, and the island drift velocity direction swung around to remain parallel to the changing isobar pattern.

In the example of these three days, the 70m mean absolute current always provides some component of flow toward the center of the low. The 40m current had a component outward from the low. Such a result is in accord with the simple Ekman current system theory.

It is interesting to note that a similar result has been obtained

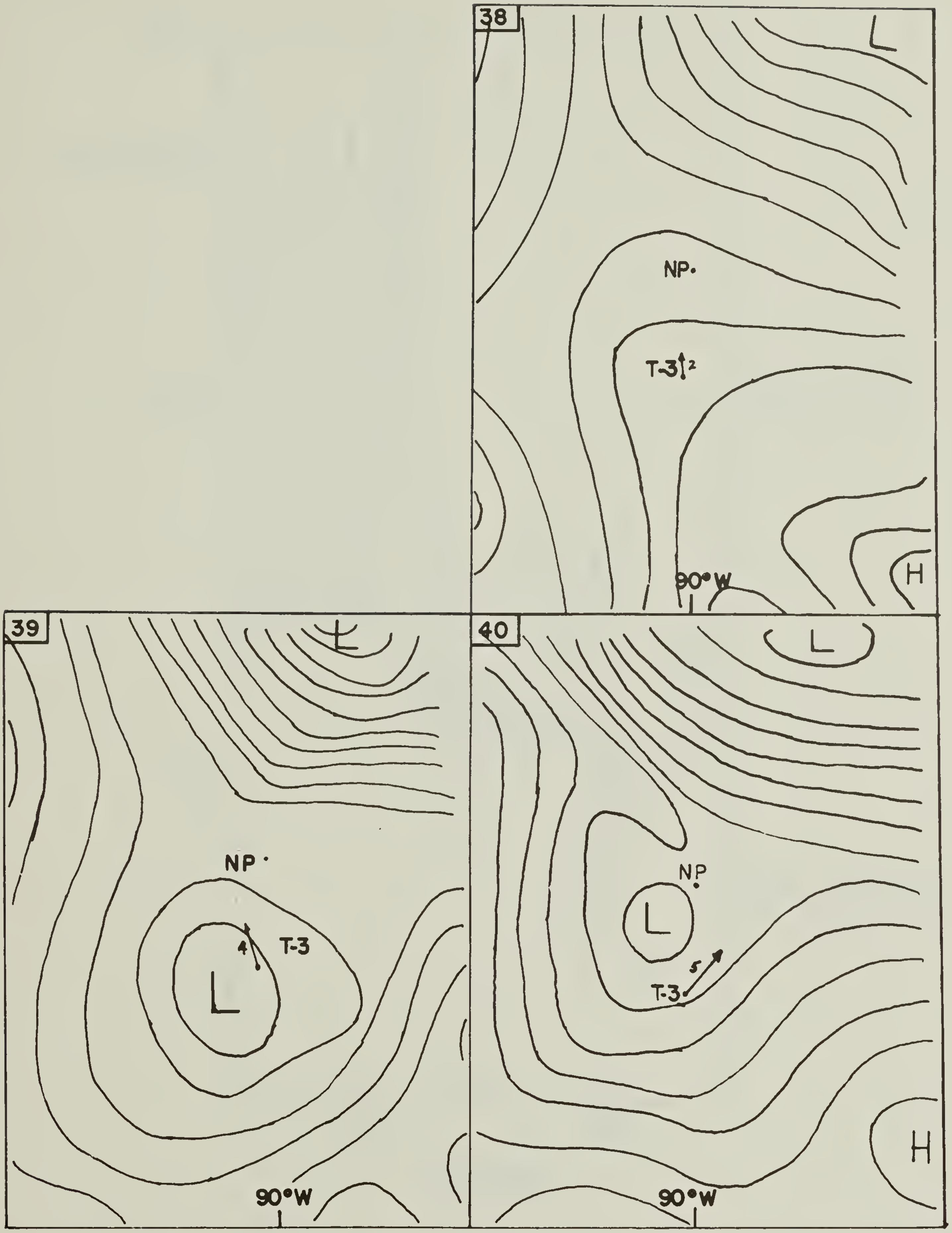

Fig. 30. U.S. Weather Bureau daily sea level pressure charts for days 38, 39, 40 (after 25 Nov 1970) of the experiment. Isobars are drawn with 4 millibar increments. North Pole, 90° W longitude, and T-3 position (85° N, 95° W) are plotted. T-3's daily drift vector shown, with numerals indicating drift rate in km/day. Drift vector tends to remain parallel to isobars.

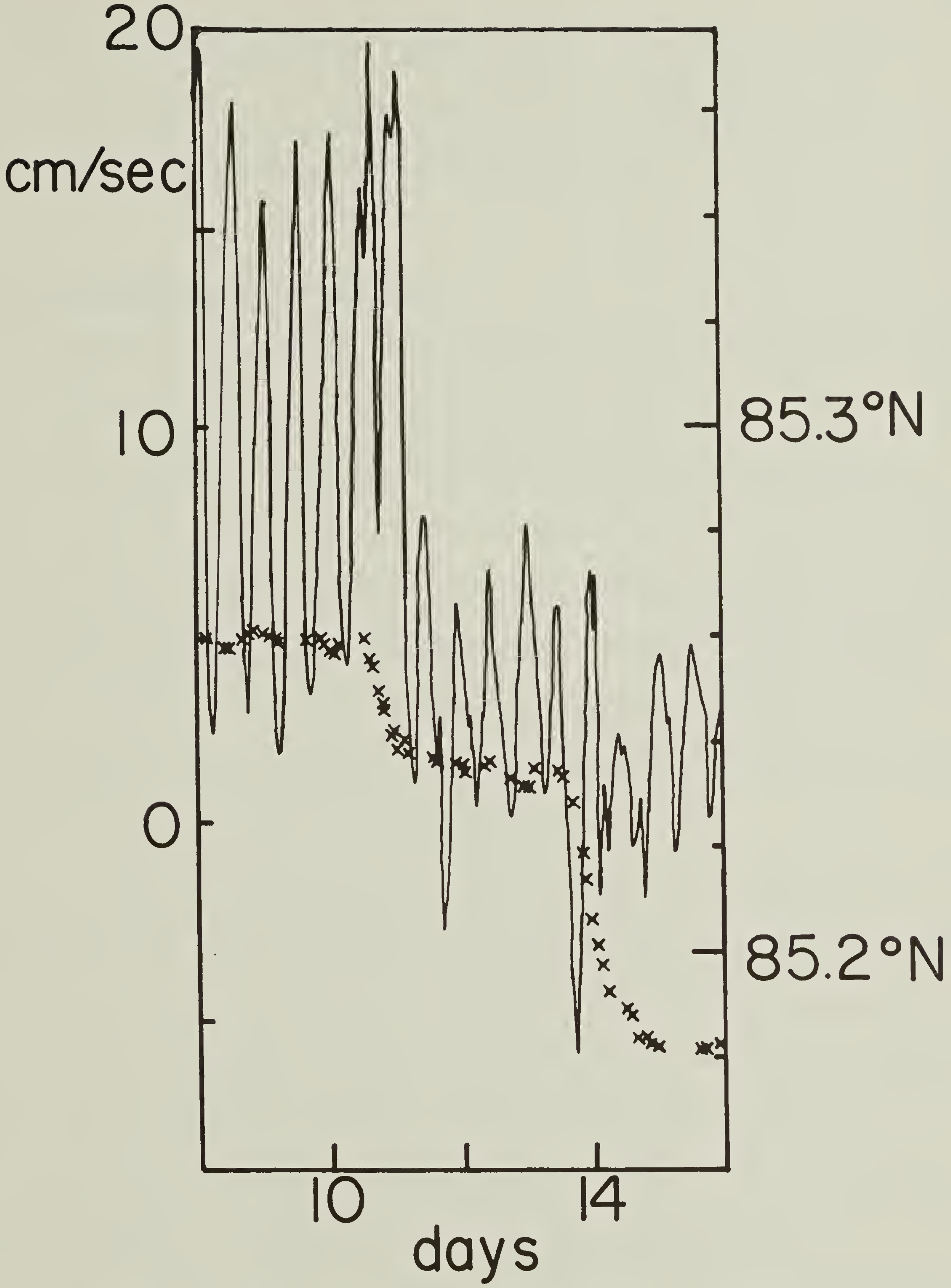

Fig. 31. Detail of 70m absolute current, north component (solid line). Time is in days from 0000Z 25 Nov 1970. Latitude from satellite fixes also plotted (crosses). Note that inertial oscillation pattern only changes at times of ice displacement.

once before. BROWNE and CRARY (1958) placed a drogue-type current meter at 150m below T-3 in 1952, and saw a flow at this depth in a direction toward lower pressure on weather charts.

Details of Inertial Current Motion

The proper identification must be made of the 12 hour oscillations which are most prominent in the 70m currents (figure 14). The only justification so far offered for identifying these oscillations as inertial currents has been that their period is very close to the local 12 hour inertial period. But are these oscillations inertial currents or semi-diurnal tides? A semi-diurnal tidal current having a period of 12 hours 25 minutes would be nearly indistinguishable from an inertial current at high latitudes. Several pieces of evidence point to the inertial character of the oscillations.

1. The intermittent, transient nature of the oscillations, is closely associated with variations in the wind and ice motion (HUNKINS, 1967). The phase and amplitude of the oscillations change abruptly with onset of ice movement. This is clearly illustrated by the detailed examination of absolute current before, during, and after a particular ice displacement event (figure 31). Thus oscillations show no change in phase or amplitude until the ice actually moves.

2. The different character of the oscillations in and below the upper mixed layer tends to eliminate the possibility of the barotropic tide, which would have uniform current velocity at all depths.

3. Free internal waves of semi-diurnal period are not allowable above latitude of 72°, because their frequency is then less than the local inertial frequency. Free internal waves are restricted to the

frequency band between the inertial and the Vaisala frequencies.

4. Surface tides at Arctic Ocean coasts are small. At Barrow, Alaska, the tidal amplitude is less than 15 cm. Barrow has an offshore shelf which would tend to amplify the tide. Tides in the deep Arctic Ocean may only be on the order of a few centimeters in height, with associated currents reaching perhaps a small fraction of a centimeter per second.

5. Although the time series length of 70 days collected in this experiment does not allow sufficient resolution, all power spectra show the inertial peak centered more on the local inertial frequency, than on the semi-diurnal tidal frequency.

The five abovementioned points may be taken as strong evidence for the inertial character of the 12 hour oscillations.

The dependence of inertial currents on the ice displacement as illustrated in figure 31, points to the local generation at the surface of these currents. POLLARD and MILLARD (1970) came to a similar conclusion from examination of current and wind records from the Atlantic Ocean.

The inertial currents observed on record C70 (figure 14) remain mostly constant in amplitude, phase and frequency during intervals of no ice movement. Comparing the oscillations before and after various similar ice motion events, sometimes they are built up, sometimes almost destroyed.

The Pollard solution for inertial currents (Equations 7,8) depends primarily on T, the duration of surface stress, in comparison with the inertial period. If T equals the inertial period, the

solution gives zero inertial current amplitude. This can be understood physically as follows: during the first half of the inertial period, inertial motion is built up moving down wind, then the current begins to turn, and by time $T/2$, has begun to head upwind. If the stress persists in the same direction during the second half of the inertial period, the stress will knock down any inertial current built up during the first half.

Stress durations equal to an integral number of inertial periods yield no inertial current if no such current existed prior to the onset of the stress. Suppose an inertial current of a particular phase and amplitude had existed prior to onset of a stress lasting an integral number of inertial periods. Then by linearity the inertial current would return to its initial phase and amplitude after the stress was turned off. Time changes in stress which are short compared with the inertial period are most effective in producing inertial oscillations.

The observable changes in inertial current amplitude may be attributed to differences in stress duration T, but there are difficulties in determining T from satellite navigation fixes, to the accuracy necessary. A difference of three hours in the determination of T gives very different inertial current amplitudes. Also, certain small amplitude but short time variations in ice movement might have a larger influence than a large amplitude, longer time variation, yet the short time variations can go undetected by the navigation fixes. For these reasons it has been impossible to find a meaningful relation between changes in inertial motion and ice displacement, except to say that changes only occur following ice movement.

Estimation of Surface Stress from Transient Current Decay

The rapid decay in 40m current speed following ice movement as observed in figure 14 can be used to obtain surface stress values. The simplest possible model of stress proportional to velocity gives

$$\frac{\partial v_{40}}{\partial t} = -Av_{40} = -\tau/\rho a$$

where v_{40} is the current at 40m, A is a proportionality constant, τ is the surface stress, a the thickness of the upper mixed layer, and ρ the density of seawater. Equation 13 has an exponential solution

$$v_{40} = v_0 e^{-At}$$

Values for A are obtained by plotting these transient decays which follow a number of storms on semi-log velocity versus time coordinates (figure 32). The resulting slopes provide values of A listed in Table 3. From Equation 13 $\tau = \rho A a v_{40}$, and for the average value of A from Table 3 and a characteristic $v = 10 \text{ cm sec}^{-1}$ we find $\tau \cong 0.68$ dynes/cm^2. This value is in rough agreement with ice stress values obtained by other estimates, including velocity shear measurements made in the upper few meters of water near a moving ice cover (K. HUNKINS, personal communication).

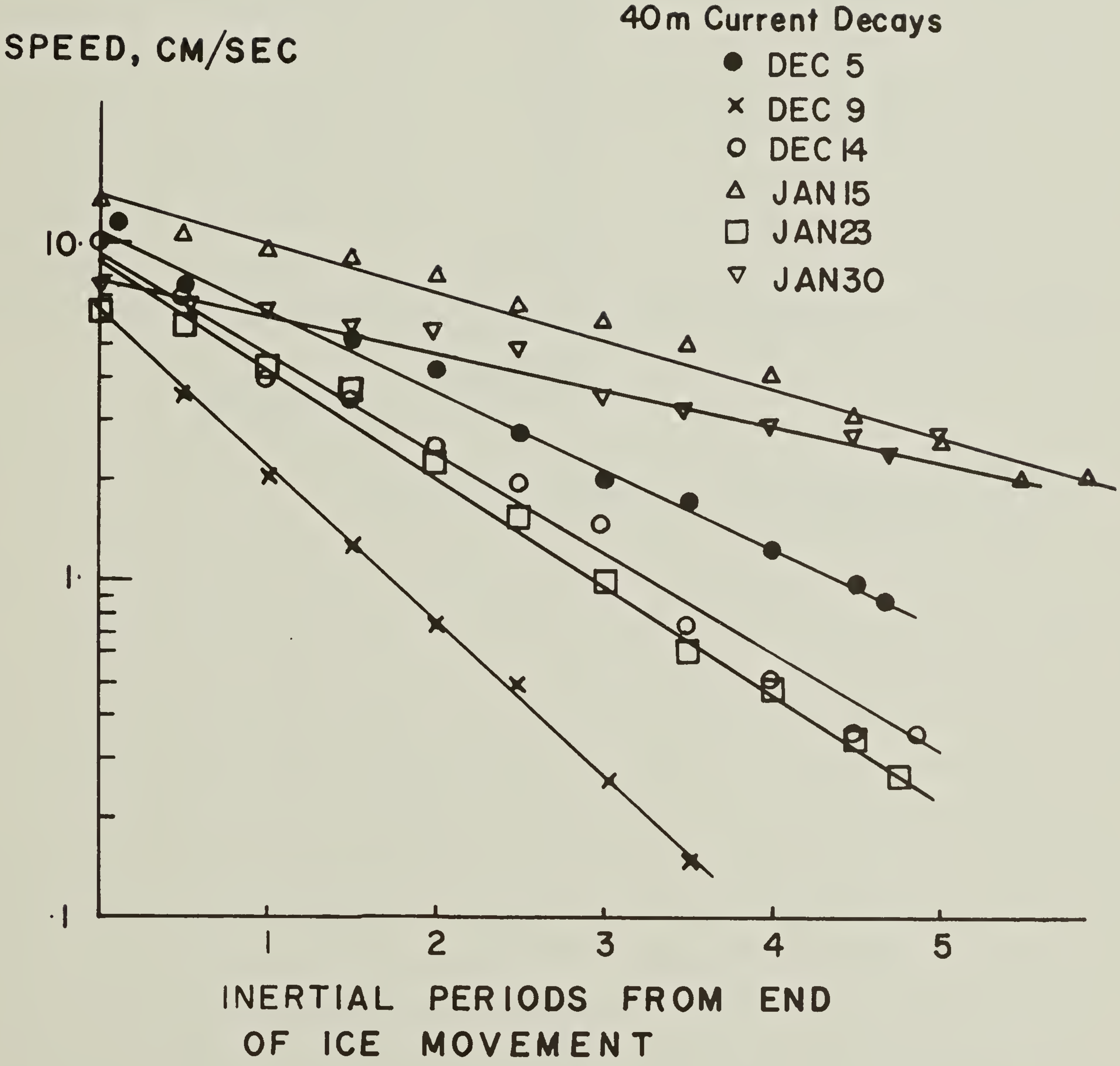

Fig. 32. Transient decay of 40m low-frequency transient current speed following end of ice displacement. Exponential character of decay shown by straight line fall-off on semi-log coordinates.

TABLE 3 Slopes From Figure 32 Giving Frictional Stress Constant A

Event	Slope θ	$\tan\theta$	$A(\sec^{-1}) = \dfrac{\tan\theta \times 2.3}{8.6 \times 10^4}$
Dec. 5	25°	.466	$1.23 \quad 10^{-5}$
Dec. 9	42°	.900	$2.38 \quad 10^{-5}$
Dec. 14	30°	.577	$1.53 \quad 10^{-5}$
Jan. 15	16°	.287	$.76 \quad 10^{-5}$
Jan. 23	33°	.649	$1.72 \quad 10^{-5}$
Jan. 30	12°	.213	$.57 \quad 10^{-5}$

$$\text{Average } A = \frac{8.19 \times 10^{-5}}{6}$$

$$= 1.36 \times 10^{-5} \sec^{-1} \left(= \frac{1}{1.7 \text{ inertial periods}}\right)$$

CONCLUSION

Energy input into the Arctic Ocean upper levels is by wind stress on the ice cover, which in turn stresses the water. The magnitude of this stress has been estimated by a new method to be about 0.7 dynes/cm^2. The surface stress varies in time in the same fashion as the synoptic weather scale. The Arctic Ocean responds to this stress with transient currents, primarily in the baroclinic mode. From current meter observations, the upper mixed layer moves often to the right, but sometimes to the left of the direction of ice displacement. A deeper layer, characterized by the 70m level, moves universally to the left of the stress direction. These observations are qualitatively in agreement with the elementary current system advanced by Ekman, and with a recent theory by Pollard.

The kinetic energy power spectrum, derived from current meter time series measurements, indicates that energy is fed in at some long period, $T > 2\text{-}3$ days. This energy probably dissipates in an energy cascade through higher frequencies, as an even fall-off of energy proportional to the -5/3 power of frequency. The even fall-off is interrupted by an energy peak at the 12 hour period, corresponding to the local inertial period. The presence of strong currents of inertial period is a resonance phenomenon associated with variable ocean currents measured on the rotating earth. These inertial currents have the form of an unmodulated sinusoid which is only significantly disturbed during the occurrence of local ice movement. Inertial currents in the upper levels of the Arctic Ocean are therefore locally generated. Attempts at more quantitative comparison of inertial current

variation with ice displacement were unsuccessful, because of insufficient resolution of the ice drift track by satellite navigation fixes. More quantitative comparison of the lower frequency transient currents will require current measurements at more depths, with closer vertical spacing between current meters.

REFERENCES

BLACKMAN, R.B. and J.W. TUKEY (1958) The measurement of power spectra from the point of view of communications engineering. Bell System Tech. Jour., 37, 185-282, 485-569.

BROWNE, I.M. and A.P. CRARY (1958) The movement of ice in the Arctic Ocean, pp. 191-209 In: Arctic sea ice, Nat. Acad. Sci. - Nat. Res. Council pub. 589, 271 pp.

CAMPBELL, W.J. (1965) The wind-driven circulation of ice and water in a polar ocean. J. Geophys. Res., 70, 3279-3301.

COACHMAN, L.K. (1969) Physical oceanography in the Arctic Ocean: 1968. Arctic, 22, 214-224.

COACHMAN, L.K. and C.A. BARNES (1961) The contribution of Bering Sea water to the Arctic Ocean. Arctic, 14, 147-161.

EKMAN, V.W. (1905) On the influence of the earth's rotation on ocean currents. Ark. f. Mat., Astron. och Fysik, 2, 1-53.

FELZENBAUM, A.I. (1958) The theory of the steady drift of ice and the calculation of the long period mean drift in the central part of the Arctic basin. Problems of the North, 2, 5-15, 13-44.

GRANGER, C.W.J., in association with M. HATANAKA (1964) Spectral analysis of economic time series. Princeton, 299 pp.

HUNKINS, K.L. (1966) Ekman drift currents in the Arctic Ocean. Deep-Sea Res., 13, 607-620.

HUNKINS, K.L. (1967) Inertial oscillations of Fletcher's Ice Island (T-3). Jour. Geophys. Res., 72, 1165-1174.

HUNKINS, K.L. (1971) Sound scattering layers in the Arctic Ocean, In: "Unpublished Report", Office of Naval Research, Code 468.

JENKINS, G.M. and T.G. WATTS (1968) Spectral analysis and its applications. Holden-Day, 525 pp.

KOLMOGOROFF, A. (1941) The local structure of turbulence in incompressible viscous fluid for very large Reynolds numbers. Dokl. Akad. Nauk SSSR, 30, 301-331.

NANSEN, F. (1902) Oceanography of the North Polar Basin. "The Norwegian North Polar Expedition 1893-96". Sci. Res., 3, Christiania.

PHILLIPS, O.M. (1971) On spectra measured in an undulating layered medium. Jour. Phys. Ocean., 1, 1-6.

POLLARD, R.T. (1970) On the generation by winds of inertial waves in the ocean. Deep-Sea Res., 17, 795-812.

POLLARD, R.T. and R.C. MILLARD, JR. (1970) Comparison between observed and simulated wind-generated inertial oscillations. Deep-Sea Res., 17, 813-821.

ROSSBY, C.G. (1938) On the mutual adjustment of pressure and velocity distributions in certain simple current systems, part II. J. Mar. Res., 1, 239-263.

VERONIS, G. and H. STOMMEL (1956) The action of variable wind stresses on a stratified ocean. J. Mar. Res., 15, 43-75.

WEBSTER, F. (1968) Observation of inertial period motions in the deep sea. Rev. Geophys., 6, 473-490.

ZUBOV, N.N. (1945) Arctic ice (Translated title). U.S. Navy Electronics Laboratory, 491 pp.

ACKNOWLEDGEMENTS

This investigation was supported by the Office of Naval Research under contract N00014-67-A-0108-0016. The Naval Arctic Research Laboratory in Barrow, Alaska, maintained the camp on T-3 and supplied other important logistical assistance. Allan Gill, Werner Tiemann, Ben Chadwick and Gary Willinski maintained the current meter array at T-3 after its installation. Programming support from Frank Malone, Stephen Teeter and Harry Demarest helped speed certain aspects of the data handling. This study was accomplished under the supervision of Dr. Kenneth L. Hunkins, whose many years of work in the Arctic led to this study as a natural outgrowth of his earlier investigations. Prof. John E. Nafe provided academic supervision. The author specifically thanks Prof. T.E. Pochapsky for instilling in him the basic desire to work in the oceans.

RECIPIENT LIST

CHIEF OF NAVAL RESEARCH CODE 415 03
OFFICE OF NAVAL RESEARCH
ARLINGTON, VIRGINIA 22217

DEFENSE DOCUMENTATION CENTER 12
CAMERON STATION
ALEXANDRIA, VIRGINIA 22314

DIRECTOR, NAVAL RESEARCH LABORATORY 06
ATTENTION TECHNICAL INFORMATION OFFICER
WASHINGTON, D. C. 20390
LIBRARY 2029 LIBRARY 2000

CHIEF OF NAVAL RESEARCH/CODE480
OFFICE OF NAVAL RESEARCH
ARLINGTON, VIRGINIA 22217

DEPARTMENT OF THE ARMY
WASHINGTON, D. C. 20315

COLD REGIONS RESEARCH & ENGINEERING
LABORATORY
POST OFFICE BOX 282
HANOVER, NEW HAMPSHIRE 03755

AIR UNIVERSITY LIBRARY
AUL3T-63-735
MAXWELL AIR FORCE BASE
ALABAMA 36112

NAVAL ACADEMY LIBRARY
ANNAPOLIS, MARYLAND 21402

DIRECTOR
NAVAL ARCTIC RESEARCH LABORATORY
BARROW, ALASKA 99723

DR. WALDO LYON
ARCTIC SUBMARINE LABORATORY
NAVAL UNDERSEA R&D CENTER
SAN DIEGO, CALIFORNIA 92132

PROF. NORBERT UNTERSTEINER
DEPT OF ATMOSPHERIC SCIENCES
UNIVERSITY OF WASHINGTON
SEATTLE, WASHINGTON 98105

EXECUTIVE DIRECTOR BRIG. H. W. LOVE
THE ARCTIC INSTITUTE OF NORTH AMERICA
SUITE 2222, TOWER A
PLACE DE VILLE
OTTAWA, ONTARIO

DR. CHARLES R. BENTLEY
GEOPHYSICAL & POLAR RESEARCH CENTER
UNIVERSITY OF WISCONSIN
6118 UNIVERSITY AVENUE
MIDDLETON, WISCONSIN 53562

DIRECTOR, INSTITUTE OF POLAR STUDIES
OHIO STATE UNIVERSITY
125 SOUTH OVAL DRIVE
COLUMBUS, OHIO 43210

MR. ROBERT C. FAYLOR
ARCTIC INSTITUTE OF NORTH AMERICA
1619 NEW HAMPSHIRE AVENUE, N. W.
WASHINGTON, D. C. 20009

MISS MARET MARTNA, DIRECTOR
ARCTIC BIBLIOGRAPHY PROJECT
406 EAST CAPITOL STREET, N. E.
WASHINGTON, D. C. 20003

LIBRARIAN
U. S. NAVAL POSTGRADUATE SCHOOL
MONTEREY, CALIFORNIA 93940

CHIEF OF NAVAL RESEARCH
OFFICE OF NAVAL RESEARCH CODE 466
ARLINGTON, VIRGINIA 22217

CHIEF OF NAVAL RESEARCH
OFFICE OF NAVAL RESEARCH CODE 468
ARLINGTON, VIRGINIA 22217

MR. BEAUMONT BUCK
DELCO ELECTRONICS
GENERAL MOTORS CORP.
6767 HOLLISTER AVENUE
GOLETA, CALIFORNIA 93107

DR. ARTHUR LACHENBRUCH
BRANCH OF GEOPHYSICS
U. S. GEOLOGICAL SURVEY
345 MIDDLEFIELD ROAD
MENLO PARK, CALIFORNIA 94025

CHIEF OF NAVAL RESEARCH CODE 480D
OFFICE OF NAVAL RESEARCH
ARLINGTON, VIRGINIA 22217

DR. KOU KUSUNOKI
POLAR RESEARCH CENTER
NATIONAL SCIENCE MUSEUM
KAGA 1-9-10, ITABASHI-KU
TOKYO, JAPAN

DR. LOUIS O. QUAM
USARP CHIEF SCIENTIST
OFFICE OF POLAR PROGRAMS
NATIONAL SCIENCE FOUNDATION
WASHINGTON, D. C. 20550

MISS MOIRA DUNBAR
DEFENCE RESEARCH BOARD/DREO
125 ELGIN STREET
OTTAWA 4, ONTARIO, CANADA

DR. A. R. MILNE
PACIFIC NAVAL LABORATORY
DEFENCE RESEARCH BOARD
DEPARTMENT OF NATIONAL DEFENCE
ESQUIMALT, BRITISH COLUMBIA, CANADA

MR. WALT WITTMANN
NAVOCEANO
CODE 8050, BLDG. 58, ROOM 206
WASHINGTON, D.C. 20390

MR. LOUIS DEGOES
EXECUTIVE SECRETARY
COMMITTEE ON POLAR RESEARCH
NATIONAL ACADEMY OF SCIENCES
2101 CONSTITUTION AVENUE, N. W.
WASHINGTON, D. C. 20418
CHIEF OF NAVAL OPERATIONS
OP-07T
DEPARTMENT OF THE NAVY
THE PENTAGON
WASHINGTON, D. C. 20350

CHIEF OF NAVAL RESEARCH/CODE484
OFFICE OF NAVAL RESEARCH
WASHINGTON, D.C. 20390

MR. M. M. KLEINERMAN
ARCTIC SCIENTIFIC PROGRAM
U. S. NAVAL ORDNANCE LABORATORY
WHITE OAK, MARYLAND 20390

MR J O FLETCHER
OFFICE OF POLAR PROGRAMS
1800 G STREET, N. W.
WASHINGTON, D. C. 20550

LIBRARIAN
WATER SECTOR LIBRARY
POLICY AND PLANNING BRANCH
DEPT OF ENERGY, MINES AND RESOURCES
OTTAWA, 3, ONTARIO
CANADA
DIRECTOR
WOODS HOLE OCEANOGRAPHIC INSTITUTION
WOODS HOLE, MASSACHUSETTS 01823

NORTHERN AFFAIRS LIBRARY
KENT-ALBERT BUILDING
OTTAWA, ONTARIO, CANADA

DR. RICHARD J. WOLD
DEPARTMENT OF GEOLOGY
UNIVERSITY OF WISCONSIN
MILWAUKEE, WISCONSIN 53201

DR. DONALD W. HOOD
INSTITUTE FOR MARINE SCIENCE
UNIVERSITY OF ALASKA
COLLEGE, ALASKA 99735

DR. LAWRENCE COACHMAN
DEPARTMENT OF OCEANOGRAPHY
UNIVERSITY OF WASHINGTON
SEATTLE, WASHINGTON 98105

DR. DAVID CLARK
DEPARTMENT OF GEOLOGY
UNIVERSITY OF WISCONSIN
MADISON, WISCONSIN 53706

OFFICE OF THE OCEANOGRAPHER
PROGRAMS DIVISION CODE N-6
732 N. WASHINGTON STREET
ALEXANDRIA, VIRGINIA 22314

DIRECTOR
OFFICE OF SCIENTIFIC INFORMATION
NATIONAL SCIENCE FOUNDATION
WASHINGTON, D. C. 20550

LIBRARIAN
DEFENCE RESEARCH BOARD OF CANADA
OTTAWA, ONTARIO, CANADA

DIRECTOR
ARKTISK INSTITUT
KRAEMERHUS
L. E. BRUUNSVEJ 10
CHARLOTTENLUND, DENMARK

DIRECTOR
NORSK POLAR INSTITUTE
MIDDLETHUNS GATE 27B
POSTBOKS 5054, MAJORSTUA
OSLO 3, NORWAY

DR. KEITH MATHER
GEOPHYSICAL INSTITUTE
UNIVERSITY OF ALASKA
COLLEGE, ALASKA 99701

CONTRACT ADMINISTRATOR
OFFICE OF NAVAL RESEARCH BRANCH OFFICE
495 SUMMER STREET
BOSTON, MASSACHUSETTS 02210

LIBRARIAN
SCOTT POLAR RESEARCH INSTITUTE
CAMBRIDGE, ENGLAND

NAVAL SHIPS SYSTEM COMMAND
ATTN CODE 205
DEPARTMENT OF THE NAVY
WASHINGTON, D.C. 20360

LIBRARIAN
TECHNICAL LIBRARY
NAVY UNDERWATER SOUND LABORATORY
FORT TRUMBULL, NEW LONDON, CONN 06320

LIBRARIAN (CODE 1640)
U.S. NAVAL OCEANOGRAPHIC OFFICE
SUITLAND, MD. 20390

LIBRARIAN
U.S. NAVAL ELECTRONICS LABORATORY CENTER
SAN DIEGO, CALIFORNIA 92152

LIBRAIAN, TECHNICAL LIBRARY
U.S.NAVAL UNDERSEA WARFARE CENTER
3202 E. FOOTHILL BLVD.
PASADENA, CALIFORNIA 91107

LIBRARIAN, TECHNICAL LIBRARY DIVISION
NAVAL CIVIL ENGINEERING LABORATORY
PORT HUENEME, CALIFORNIA 93041

DR. JOHANNES WILJHELM
DET DANSKE METEOROLOGISK INSTITUT
GAMLEHAVE ALLE 22
CHARLOTTENLUND, DENMARK

DR. ALBERT H. JACKMAN
CHAIRMAN DEPT OF GEOGRAPHY
WESTERN MICHIGAN UNIVERSITY
KALAMAZOO, MICHIGAN 49001

DR WARREN DENNER
CODE 58DW
DEPARTMENT OF OCEANOGRAPHY
NAVAL POSTGRADUATE SCHOOL
MONTEREY, CALIFORNIA 93940

DIRECTOR, U S NAVAL RESEARCH LABORATORY 06
WASHINGTON, D. C. 20390
ATTN LIBRARY CODE 2029 (ONRL)

OFFICE OF NAVAL RESEARCH RES REP
COLUMBIA UNIVERSITY
LAMONT - DOHERTY GEOLOGICAL OBSERVATORY
TORREY CLIFF, PALISADES, NEW YORK 10964

DR. RITA HORNER
INSTITUTE OF MARINE SCIENCES
UNIVERSITY OF ALASKA
COLLEGE, ALASKA 99701

DR. KNUT AAGAARD
DEPT. OF OCEANOGRAPHY
UNIVERSITY OF WASHINGTON
SEATTLE, WASHINGTON 98105

PROF. CLARENCE CLAY
GEOPHYSICAL & POLAR RESEARCH CENTER
6118 UNIVERSITY AV.
MIDDLETON, WIS 53562

PROF. WILLIAM MCINTIRE
COASTAL STUDIES INSTITUTE
LOUSIANA STATE UNIVERSITY
BATON ROUGE, LOUSIANA 70803

DR. J. A. GALT
DEPT. OF OCEANOGRAPHY
NAVAL POST GRADUATE SCHOOL
MONTEREY, CALIFORNIA 93940

DR. WESTON BLAKE, JR.
GEOLOGICAL SURVEY OF CANADA
DEPT. OF ENERGY, MINES & RESOURCES
601 BOOTH STREET
OTTAWA 4, ONTARIO

CHIEF SCIENTIST
ONR BRANCH OFFICE CHICAGO
536 SOUTH CLARK STREET
CHICAGO, ILLINOIS 60605

CHIEF SCIENTIST
ONR BRANCH OFFICE, PASADENA
1030 EAST GREEN STREET
PASADENA, CLAIFORNIA 91101

DIRECTOR OF DEFENSE RESEARCH AND ENGINEERING
OFFICE OF THE SECRETARY OF DEFENSE
WASHINGTON D C 20301
ATTN: OFFICE ASST. DIRECTOR (RESEARCH)

OFFICE OF NAVAL RESEARCH 2
DEPT OF NAVY
WASHINGTON D C 20360
CODE 460
410

Unclassified
Security Classification

DOCUMENT CONTROL DATA - R & D

(Security classification of title, body of abstract and indexing annotation must be entered when the overall report is classified)

1. ORIGINATING ACTIVITY (Corporate author)
Lamont-Doherty Geological Observatory
of Columbia University

2a. REPORT SECURITY CLASSIFICATION
Unclassified

2b. GROUP
Arctic Group

3. REPORT TITLE
Observations of Currents in the Arctic Ocean

4. DESCRIPTIVE NOTES (Type of report and inclusive dates)
Technical Report

5. AUTHOR(S) (First name, middle initial, last name)
Robert L. Bernstein

6. REPORT DATE
January, 1972

7a. TOTAL NO. OF PAGES
79

7b. NO. OF REFS
21

8a. CONTRACT OR GRANT NO.
N-00014-67-A-0108-0016

b. PROJECT NO.
Task Number NR 307-320/1-6-69(415)

c.

d.

9a. ORIGINATOR'S REPORT NUMBER(S)
7

9b. OTHER REPORT NO(S) (Any other numbers that may be assigned this report)

10. DISTRIBUTION STATEMENT
Reproduction of this document in whole or in part is permitted for any purpose of the U. S. Government.

11. SUPPLEMENTARY NOTES

12. SPONSORING MILITARY ACTIVITY
Office of Naval Research
Washington D C

13. ABSTRACT

An array of current meters was installed and operated for three months at Ice Island T-3, at 85°N, 95°W in the Arctic Ocean. Current meters were placed at three sites at 40m and 70m depths, with signal outputs all wired to a common recording system. The drift motion of T-3 can be eliminated from the records using frequent precise satellite navigation fixes. All records show predominant 12 hour period inertial currents, superimposed on lower frequency transient currents, which occur during intervals of rapid ice drift. The transient currents, at 40m in an upper layer veer to the right of the ice drift direction, while currents in the lower layer at 70m veer to the left. The observed ice drift and currents are consistent with the theory of elementary currents first advanced by Ekman, and with a recent theory by Pollard.

The inertial currents have constant phase and amplitude which only change during intervals of ice displacement, suggesting the local generation of these currents in the upper levels of the ocean.

The kinetic energy power spectrum derived from the current meter time series shows an even fall-off of energy proportional to the -5/3 power of frequency. This fall-off is interrupted by an energy peak at the 12 hour inertial period. The -5/3 fall-off suggests that energy is fed in at large scales and long periods (>2-3 days) and dissipates in an energy cascade through smaller scales and high frequencies.

(continued overleaf)

Unclassified
Security Classification

The magnitude of the surface stress which the moving ice cover exerts on the underlying ocean has been estimated by a new method. From the decay of transient currents under a non-moving ice cover, a simple theory gives a stress value around 0.7 dynes/cm^2, for 10 cm/sec of relative velocity between the ice and the water underneath.

14. KEY WORDS	LINK A		LINK B		LINK C	
	ROLE	WT	ROLE	WT	ROLE	WT
Arctic Ocean						
Ocean currents						
Inertial motion						
Ice drift						

DD FORM 1 NOV 65 1473 (BACK)
(PAGE 2)

Unclassified
Security Classification